NEW METHODS FOR DETERMINING THE COMPLEX PERMITTIVITY OF DIFFERENT GLUCOSE CONCENTRATIONS BY WAVEGUIDE AND ANTENNA MEASUREMENTS AT V-BAND

TELECOMMUNICATIONS ENGINEERING

Author: Helena Cano García

Supervisors of the thesis: Panos Kosmas and Themos Kallos

Year: September 2013

ACKNOWLEDGMENTS

First of all I wish to thank my thesis' supervisors Drs. Panos Kosmas and Themos Kallos for giving me the opportunity to work in this interesting project. Furthermore, I wish to thank them for all their support, guidance and encouragement that have helped me to finish successfully this thesis.

Thank you to the International Relations team from the ETSETB of the Universitat Politècnica de Catalunya for giving me this opportunity and for the help provided.

A big thank you to my parents, my grandparents and my two charming brothers, thanks to all them for their unconditional and unique support during all my degree and for their help and comprehension in all the good and bad moments.

At last but not at least, I would like to thank my friends in Barcelona and London for all the enjoyable moments that have made the black days of this degree more bearable.

TABLE OF CONTENTS

LIST OF FIGURES

LIST OF TABLES

ABSTRACT

Diabetes is a metabolic disease that affects millions of people in the world. To control the status of this disease, diabetic patients have to measure continuously their glucose levels during all day. Nowadays, the method to monitor the glucose content in blood is called finger prick test. This method is very accurate, but it is also painful and invasive and, over the long term, it can damage the finger tissue. For this reason, this thesis presents two new and non-invasive methods to determine the glucose content in blood without any harmful effect.

These new methods present two different forms to detect the glucose content using microwaves. The first method is based in a waveguide structure consisting of two waveguides and a tank containing the sample between them. The second method uses a similar structure to the first method, but instead of using waveguides, it uses antennas.

To study both methods the CST simulation software package has been used. CST's versatility allowed us to perform various realistic electromagnetic (EM) simulations and extract the desired S-parameters for each scenario.

The analysis of the first method has shown that the simulation results and the experimental results are really similar. This first analysis has also shown that plane waves propagation is necessary in order to apply the post processing analysis employed in this work.

To satisfy the plane wave requirement, a second setup based on antennas in the far field has been used. In this case, the results of the post processing part were not as good as expected. This might result from the association of the TRL calibration and NRW algorithm for fulfil the plane wave requirement. For this reason, further analysis involving the development of our own calibration procedure will be required.

RESUM

La diabetis és una malaltia metabòlica que afecta a gran part de la població mundial. Per tal de controlar l'estat de la malaltia, totes aquelles persones que la pateixen han de controlar els seus nivells de glucosa constantment. Actualment, el mètode utilitzat per la monitorització del contingut de glucosa en la sang està basat en una tècnica invasiva anomenada punció digital. Aquest mètode determina la quantitat de glucosa amb precisió. Tot i així, és un mètode dolorós que amb el seu ús reiterat pot danyar el teixit de la zona on es realitza la punció. Per intentar evitar això, aquest projecte presenta dos nous mètodes per poder detectar els nivells de glucosa de manera no invasiva i, d'aquesta manera, evitar els problemes derivats de la utilització de la punció digital.

El dos nous mètodes tractats en aquest projecte presenten dues maneres diferents de detectar els nivells de glucosa de manera no invasiva utilitzant microones. El primer mètode estudiat utilitza una estructura composta per dues guies de ona i un contenidor amb la mostra situat entre elles. El segon mètode, utilitza una estructura similar a la del primer mètode, però en aquest cas, les guies d'ona son substituïdes per dues antenes.

Per estudiar els dos mètodes, s'ha utilitzat un software de simulació anomenat CST que permet l'estudi dels paràmetres S i dels diferents camps electromagnètics.

Després de l'anàlisi del primer mètode, s'ha demostrat que les simulacions presenten resultats similars als resultats de l'experiment realitzat prèviament per MediWiSe. Amb aquest primer anàlisis, també s'ha demostrat que per poder utilitzar les tècniques de post processat (TRL i NRW) és necessari utilitzar ones planes.

Finalment, per tal d'aconseguir ones planes es va decidir utilitzar la segona estructura basada en antenes, però tot i que s'esperava que els resultats del post processat fossin bons, els resultats obtinguts no acaben de ser satisfactoris. Això pot ser degut al fet de que no es compleix el requeriment d'ones planes necessari per aplicar la calibració TRL i l'algoritme NRW. Per això, de cara al futur, es proposa realitzar un calibratge propi que solucioni aquesta problemàtica.

RESUMEN

La diabetes es una enfermedad metabólica que afecta a gran parte de la población mundial. Para poder controlar el estado de la enfermedad, los pacientes deben controlar continuamente sus niveles de glucosa durante el todo día. Actualmente, el método utilizado para la monitorización del contenido de glucosa en la sangre, está basado en una técnica invasiva llamada punción digital. Este método determina la cantidad de glucosa con precisión. Sin embargo, es un método doloroso y su uso reiterado puede dañar el tejido de donde se realiza la punción. Por ello, este proyecto presenta dos nuevos métodos para poder detectar los niveles de glucosa de manera no invasiva y, por lo tanto, evitando los problemas derivados del uso de la punción digital.

Los dos nuevos métodos tratados en este proyecto, presentan dos maneras diferentes de detectar los niveles de glucosa de manera no invasiva utilizando frecuencias de microondas. El primer método utiliza una estructura compuesta por dos guías de onda y un contenedor con la muestra situado entre ellas. El segundo método utiliza una estructura similar a la del primer método, pero en este caso se emplean antenas en vez de guías de onda.

Para estudiar ambos métodos se ha usado un software de simulación llamado CST que permite el estudio de los parámetros S y los diferentes campos electromagnéticos.

Tras el análisis del primer método, se ha demostrado que las simulaciones presentan resultados similares a los resultados de los experimentos previos realizados por MediWiSe. Tras este primer análisis también se puede concluir que para el uso de nuestras técnicas de post procesado (TRL y NRW) es necesario el uso de ondas planas.

Por otro lado, en el estudio de la estructura basada en antenas, aunque se esperaba que los resultados del post procesado fueran buenos, los resultados que se obtienen no acaban de ser satisfactorios. Esto puede ser debido al hecho de que no se cumple el requisito de tener ondas planas necesario para aplicar la calibración TRL y el algoritmo NRW. Por esta razón, de cara al futuro se propone realizar una calibración propia que solvente estos problemas.

1. INTRODUCTION

1.1. CONTEXT OF THE PROJECT

Diabetes mellitus is a chronic disease that occurs when the body cannot produce enough insulin or cannot use it effectively [1]. As a result, diabetic persons do not absorb glucose properly and they suffer from hyperglycaemia, which means that the glucose is not absorbed by the cells and stays circulating in the blood damaging tissues.

This metabolic disease can lead to serious health problems over time, including diabetic retinopathy (a leading cause of blindness and visual disability), kidney failure, heart failure and peripheral neuropathy associated with limb pain, poor circulation, gangrene and subsequent amputation [2].

Diabetes is a growing problem worldwide that affects more than the 8.3% of the world population. The number of cases is increasing every year and by 2030 it is expected that, this metabolic disease, will affect to the 12.3% of the world population [3]. This growing number of diabetic cases is due to the world's increasingly aging population, increasingly unhealthy diets, sedentary lifestyles and obesity [4].

For diagnostic and treatment of diabetes, is important to determine the glucose concentration in blood in the most accurate way. Nowadays, the most common method for providing knowledge of the patient's glucose level is based on a painful, invasive technique, called finger prick test. Through this process, the patient has to be subjected to small and painful injuries several times in a day. Furthermore, the use of this technique has the risk of infection and, over the long term, can damage the finger tissue. For these reasons, a significant amount of research effort is dedicated to develop different non-invasive and non-painful technologies to monitor the glucose levels.

In the past decades, some non-invasive studies have been done based on ultrasound and optical techniques. However, none of these techniques have been able to replace the finger prick test due to accuracy and reliability problems [5] [6]. Currently, some measurement techniques at microwave frequencies are being investigated and it seems that these microwave techniques would have better results than the previous techniques.

This thesis will focus on the simulation of non-invasive microwave measurement techniques using two different structures, a waveguide structure and an antenna structure. To perform the simulations of both structures, CST software has been used.

CST is an electromagnetic (EM) simulation software. It is useful for the design and optimization of devices operating in a wide range of frequencies, including microwave frequencies. This software is capable of simulating numerous designs, as well as being able to calculate the S-parameters and the effects of EM fields on diverse substances.

1.2. OBJECTIVES

The objective of this dissertation is to study and evaluate two different non-invasive microwave measurement techniques, the waveguide structure and the antenna structure. Furthermore, another important objective is to extract the permittivity and permeability form different glucose solutions using a specific frequency range and structure and post processing techniques. To reach these objectives, different CST simulations, using two different non-invasive methods, have been done.

The first non-invasive method, which is based on a waveguide structure, is a replication of an experiment did by MediWiSe. Therefore, in this case, the evaluation of the technique is going to be based in the comparison between the simulation results and the experimental results. For this structure, to extract the permittivity and permeability specific post processing techniques (Section 2.5) are going to be used.

The second non-invasive method is based on an antenna structure, and in this case, the objective is to extract the dielectric and magnetic constants using the same post processing as in the first method. Moreover, in this case, the evaluation of this technique is going to be done using a comparison between the sensitivity of the waveguide structure and the sensitivity of the antenna structure.

1.3. THESIS STRUCTURE

This project is organized in different chapters. After the introduction in this chapter, Chapter 2 is will introduce some necessary concepts to understand the experimental part. This chapter will also present the state of the art of the millimetre waves, as well as a brief introduction to

the waveguide theory, the antenna theory and the post processing methods used in the experiment.

The third and the fourth chapter will focus on the simulations with CST and the different results obtained. These chapters will present the simulation setup and the results of different simulations for two different structures, the waveguide and antenna structure respectively.

Finally, after the analysis of the results, there are two more chapters. The fifth chapter will present the conclusions of the whole thesis and the chapter six is going to expose the future work.

2. BACKGROUND

2.1. MILLIMETER WAVE SENSING

Millimeter waves are waves that operate between 30 GHz and 100 GHz. This frequency range has been used in multiple sensors for different proposes. Including estimating the permeability and permeability of different substances, namely building materials [7][8], aqueous solutions [9], oils [10] and glucose solutions [11].

This dissertation will focus in the use of millimeter waves to determine the permittivity and permeability of different glucose solutions. This method can be used to sense glucose changes in blood because an alteration in glucose levels affects the electrical properties of blood and subcutaneous tissue at microwave frequencies [12].

2.2. WAVEGUIDE THEORY

This section reviews the background waveguide theory and focuses on the specific case of rectangular waveguides used in this project. The first section, Section 2.2.1., presents a brief introduction on the basic concepts of waveguides. Then, the second section, Section 2.2.2., presents the waveguide theory associated with the hollow rectangular waveguides, which are going to be used in the simulations.

2.2.1. INTRODUCTION

Waveguides are transmission mediums used to guide electromagnetic waves from one point in space to another in an efficient way. These transmission mediums are useful at microwave frequencies because they present a low-loss transmission at these frequencies. Furthermore, waveguides are valuable because they have high power-handling capability and low loss but are bulky and expensive [13].

Waveguides can be generally classified as parallel plate waveguides, rectangular waveguides or circular and elliptical waveguides. Waveguide selection is usually based on the desired

operating frequency band, the amount of power that is going to be transferred and the amount of transmission losses that can be tolerated.

2.2.2. RECTANGULAR WAVEGUIDES

Rectangular waveguides is one of the earliest types of transmission lines used to transport microwaves. This kind of waveguides has typically a hollow conductor structure and it can propagate infinite number of transverse electric (TE) or transverse magnetic (TM) modes, but not transverse electromagnetic (TEM) modes because it is made with only one conductor [14].

The geometry of this type of waveguides can be seen in (Fig. 2.1).

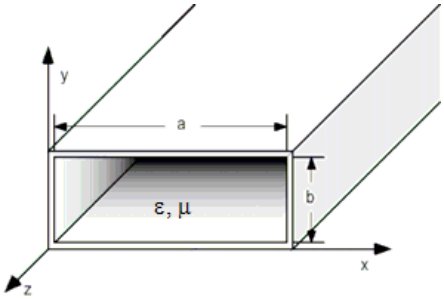

FIGURE 2.1: RECTANGULAR WAVEGUIDE GEOMETRY

For the study of rectangular waveguides, it can be supposed that a ≥ b and that the guide is filled with a dielectric material with ε and μ values. Depending on the a and b values, the waveguide would propagate TE or TM modes. Furthermore, for rectangular waveguides, the fact that a > b allows a single mode operation.

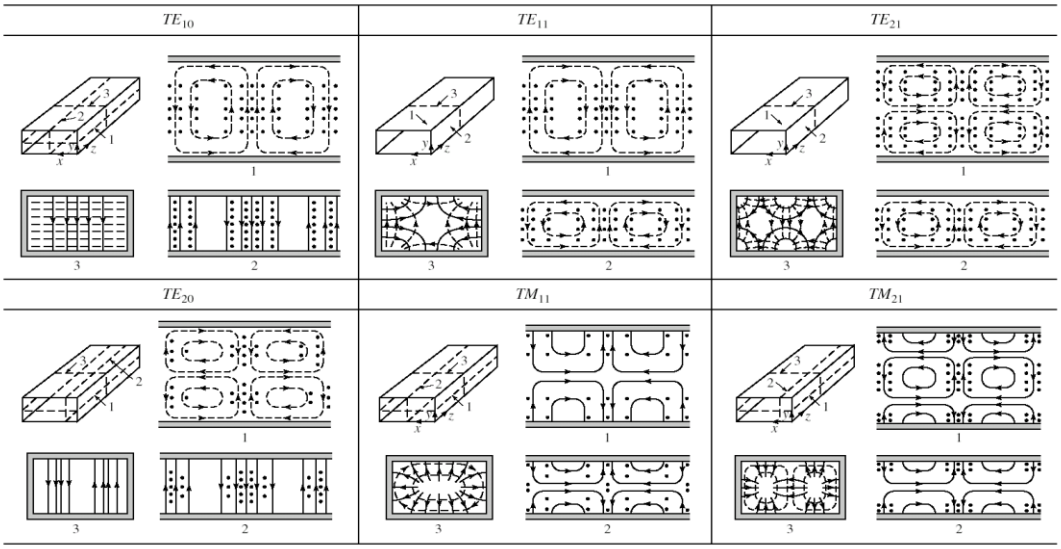

FIGURE 2.2: FIELD LINES FOR SOME OF THE LOWER ORDER MODES OF A RECTANGULAR WAVEGUIDE [15]

TRANSVERSE ELECTRIC (TE)

TE modes are characterized by electric field axial component, E_z, zero, while magnetic field axial component, H_z, must satisfy the reduced wave equation [14]:

$$\left(\frac{\partial^2}{\partial x^2}+\frac{\partial^2}{\partial y^2}+k_c^2\right)h_z(x,y)=0 \tag{2.1}$$

where:

$h_z(x,y)=H_z(x,y,z)\,e^{j\beta z}$ and $k_c^2=k^2-\beta^2$ is the cut-off wavenumber.

The solution to the equation (Eq. 2.1) for H_z can be found using differential equations theory. The detailed process to achieve the following solution could be found in [14].

$$H_z(x,y,z)=A_{mn}\cos\left(\frac{m\pi x}{a}\right)\cos\left(\frac{n\pi y}{b}\right)e^{-j\beta z} \tag{2.2}$$

where A_{mn} is an arbitrary amplitude constant.

For a rectangular waveguide, the solutions of the transverse field components (H_x, H_y, E_x and E_y) of the TE_{mn} mode can be found using the solution for H_z (Eq. 2.2) and Maxwell equations [14].

$$H_x=\frac{-j\beta}{k_c^2}\frac{\partial H_z}{\partial x} \quad\rightarrow\quad H_x=\frac{j\beta m\pi}{k_c^2 a}A_{mn}\sin\left(\frac{m\pi x}{a}\right)\cos\left(\frac{n\pi y}{b}\right)e^{-j\beta z} \tag{2.3}$$

$$H_y=\frac{-j\beta}{k_c^2}\frac{\partial H_z}{\partial y} \quad\rightarrow\quad H_y=\frac{j\beta n\pi}{k_c^2 b}A_{mn}\cos\left(\frac{m\pi x}{a}\right)\sin\left(\frac{n\pi y}{b}\right)e^{-j\beta z} \tag{2.4}$$

$$E_x=\frac{-j\omega\mu}{k_c^2}\frac{\partial H_z}{\partial y} \quad\rightarrow\quad E_x=\frac{j\omega\mu n\pi}{k_c^2 b}A_{mn}\cos\left(\frac{m\pi x}{a}\right)\sin\left(\frac{n\pi y}{b}\right)e^{-j\beta z} \tag{2.5}$$

$$E_y=\frac{j\omega\mu}{k_c^2}\frac{\partial H_z}{\partial x} \quad\rightarrow\quad E_y=\frac{-j\omega\mu n\pi}{k_c^2 a}A_{mn}\sin\left(\frac{m\pi x}{a}\right)\cos\left(\frac{n\pi y}{b}\right)e^{-j\beta z} \tag{2.6}$$

For this case, the propagation constant is:

$$\beta=\sqrt{k^2-k_c^2}=\sqrt{k^2-\left(\frac{m\pi}{a}\right)^2-\left(\frac{n\pi}{b}\right)^2} \tag{2.7}$$

The m refers to the number of half cycle variations of the x direction fields, and the n denotes the number of half cycle variations of the y direction fields. Each m and n combination defines one operation mode, TE_{mn}, and each mode has a cutoff frequency.

$$f_{c_{mn}} = \frac{k_c}{2\pi\sqrt{\mu\varepsilon}} = \frac{1}{2\pi\sqrt{\mu\varepsilon}}\sqrt{\left(\frac{m\pi}{a}\right)^2 + \left(\frac{n\pi}{b}\right)^2} \tag{2.8}$$

The mode with the lowest cutoff frequency is known as the dominant mode. Therefore, for TE modes, TE_{10} is the dominant mode for a waveguide with a > b [16].

TRANSVERSE MAGNETIC MODES (TM)

TM modes are characterized by magnetic field axial component, H_z, zero, while electric field axial component, E_z, must satisfy the reduced wave equation [14]:

$$\left(\frac{\partial^2}{\partial x^2} + \frac{\partial^2}{\partial y^2} + k_c^2\right) e_z(x,y) = 0 \tag{2.9}$$

where:

$e_z(x,y) = E_z(x,y,z)e^{j\beta z}$ and $k_c^2 = k^2 - \beta^2$ is the cut-off wavenumber.

This equation (Eq. 2.9) can be solved using the separation of variables procedure. The detailed process to achieve the following solution could be found in [14]. The solution of (Eq. 2.9) is:

$$E_z(x,y,z) = B_{mn}\sin\left(\frac{m\pi x}{a}\right)\sin\left(\frac{n\pi y}{b}\right)e^{-j\beta z} \tag{2.10}$$

As in the TE modes, in this case the solutions of H_x, H_y, E_x, E_y can be found using the solution for E_z.

$$H_x = \frac{j\omega\varepsilon}{k_c^2}\frac{\partial E_z}{\partial y} \quad \rightarrow \quad H_x = \frac{j\omega\varepsilon n\pi}{k_c^2 a}B_{mn}\sin\left(\frac{m\pi x}{a}\right)\cos\left(\frac{n\pi y}{b}\right)e^{-j\beta z} \tag{2.11}$$

$$H_y = \frac{-j\omega\varepsilon}{k_c^2}\frac{\partial E_z}{\partial x} \quad \rightarrow \quad H_y = \frac{-j\omega\varepsilon n\pi}{k_c^2 b}A_{mn}\cos\left(\frac{m\pi x}{a}\right)\sin\left(\frac{n\pi y}{b}\right)e^{-j\beta z} \tag{2.12}$$

$$E_x = \frac{-j\beta}{k_c^2}\frac{\partial E_z}{\partial x} \quad \rightarrow \quad E_x = \frac{-j\beta m\pi}{k_c^2 b}A_{mn}\cos\left(\frac{m\pi x}{a}\right)\sin\left(\frac{n\pi y}{b}\right)e^{-j\beta z} \tag{2.13}$$

$$E_y = \frac{j\omega\mu}{k_c^2}\frac{\partial E_z}{\partial y} \quad \rightarrow \quad E_y = \frac{-j\omega\mu n\pi}{k_c^2 a}A_{mn}\sin\left(\frac{m\pi x}{a}\right)\cos\left(\frac{n\pi y}{b}\right)e^{-j\beta z} \tag{2.14}$$

As for TE modes, the propagation constant and the cutoff frequency are:

$$\beta = \sqrt{k^2 - k_c^2} = \sqrt{k^2 - \left(\frac{m\pi}{a}\right)^2 - \left(\frac{n\pi}{b}\right)^2} \tag{2.15}$$

$$f_{c_{mn}} = \frac{k_c}{2\pi\sqrt{\mu\varepsilon}} = \frac{1}{2\pi\sqrt{\mu\varepsilon}}\sqrt{\left(\frac{m\pi}{a}\right)^2 + \left(\frac{n\pi}{b}\right)^2} \tag{2.16}$$

The mode with the lowest cutoff frequency for TM modes is the TM_{11} because in rectangular waveguides with TM modes m and n cannot be zero. Therefore, TM_{00}, TM_{01} and TM_{10} do not exist [17].

2.2.3. POWER TRANSMISSION AND ATTENUATION

The total power transmitted, power flow, for the waveguide along the waveguide direction is obtained by integrating the z component of the Poynting vector over the cross-sectional area of the guide [16].

$$P_T = \int_S \mathcal{P}_z \, dS \tag{2.17}$$

where $\mathcal{P}_z$ is the Poynting vector, and it can be written as:

$$\mathcal{P}_z = \frac{1}{2} Re(\bar{E} \times \overline{H^*})\hat{z} \tag{2.18}$$

In the specific case of the TE_{10} mode, the power flow can be calculated as follows [14]:

$$\begin{aligned} P_{10} &= \frac{1}{2} Re\left(\int_{x=0}^{a}\int_{y=0}^{b} \bar{E} \times \overline{H^*} \cdot \hat{z}\, dxdy\right) = \frac{1}{2} Re\left(\int_{x=0}^{a}\int_{y=0}^{b} E_y H_y^*\, dydx\right) = \\ &= \frac{\omega\mu a^2}{2\pi^2} Re(\beta)|A_{10}|^2 \int_{x=0}^{a}\int_{y=0}^{b} \sin^2\frac{\pi x}{a} dydx = \frac{\omega\mu a^3}{2\pi}|A_{10}|^2\, b\, Re(\beta) \end{aligned} \tag{2.19}$$

The attenuation in rectangular waveguides can be due to dielectric losses or conduction losses is [18]:

$$\alpha = \alpha_d + \alpha_c \tag{2.20}$$

where α_d and α_c are the attenuation constants due to dielectric and conduction losses respectively.

The dielectric losses, α_d, can be characterized by the loss tangent, $\tan\delta$ or the conductivity σ_d. And the equation of the attenuation constant can be written as follows [16]:

$$\alpha_d = \frac{\omega \, tan\delta}{2c\sqrt{1-\frac{f_c^2}{f^2}}} \tag{2.21}$$

The determination of α_c is complicated and the explanation of the procedure to determine these losses can be found in [16]. However, the general equation of these losses is:

$$\alpha_c = \frac{P_l}{2P_T} \tag{2.22}$$

where P_l is the power lost per unit length due to finite wall conductivity, and P_T is the power flow.

2.3. ANTENNA THEORY

This section reviews basic antenna theory and focuses on microstrip antennas, which are going to be used in the experimental part. In Section 2.3.1 a brief introduction to antenna theory is presented. Section 2.3.2 presents microstrip antennas. And finally, Section 2.3.3 presents different parameters of the antenna analysis.

2.3.1. INTRODUCTION

Antennas are transmitting or receiving components designed to radiate or receive electromagnetic waves. In transmission, their function is to convert the propagated wave in a transmission line to a propagated plane wave in free space. In reception, they apply the opposite conversion.

There is a wide variety of antenna geometries and types. The most common ones are wire antennas, aperture antennas, microstrip antennas and reflector antennas.

This section is going to study microstrip patch antennas, their benefits and drawbacks and their fundamental parameters.

2.3.2. MICROSTRIP ANTENNAS

Nowadays, microstrip antennas, also called patch antennas, are widely used due to their unique benefits. They are low cost, lightweight, electrically thin, easy to integrate with microwave integrated circuits, easy to feed and so on. However, these antennas suffer from various drawbacks including a narrow bandwidth, less efficiency than some other types of antennas, high feed network losses, high cross correlation, limited power capacity and tolerance problems [19][20]. Nevertheless, nowadays, some of these problems have been alleviated to some extent [21].

Microstrip antennas are a single-layer design consisting of flat parts. Usually, these flat parts are the patch, the substrate, the ground plane and the feeding part.

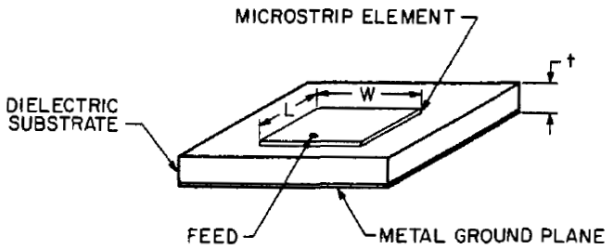

FIGURE 2.3: RECTANGULAR MICROSTRIP ANTENNA [22]

The rectangular patch layer of (Fig. 2.3) is one of the large numbers of shapes that microstrip patch antennas can adopt; however, for microwave frequencies, the most common are rectangular, square and circular patches.

These types of antennas belong to the resonant antennas class. The length, L, of the patch is called resonant length and is the most critical dimension because it determines the resonant frequency. In the specific case of a circular patch antenna, the resonance frequency varies with the radius of the patch. In addition to the length, the thickness of the substrate affects the resonance frequency and the bandwidth of the antenna. The bandwidth increases if the thickness increases but with limits, otherwise the antenna will stop resonating. Therefore, the performance of this kind of antennas is affected by the patch geometry, the substrate properties and the feed technique [23].

2.3.3. MICROSTRIP ANTENNA PARAMETERS

The following sections present the most important parameters of the antennas. These parameters are the ones that are going to be used in the experimental part (Chapter 4).

RADIATION PATTERN

The radiation pattern shows the variation of power density with angular position. The radiation pattern is a 3D graph with the power against elevation and azimuth angles. However, commonly, the radiation pattern is represented as two different 2D graphs using different plane pattern plots, the E-plane and the H-plane, where one of the angles, θ or ϕ, is held fixed while the other one varies. Therefore, using the radiation pattern is possible to know the radiation direction of the antenna.

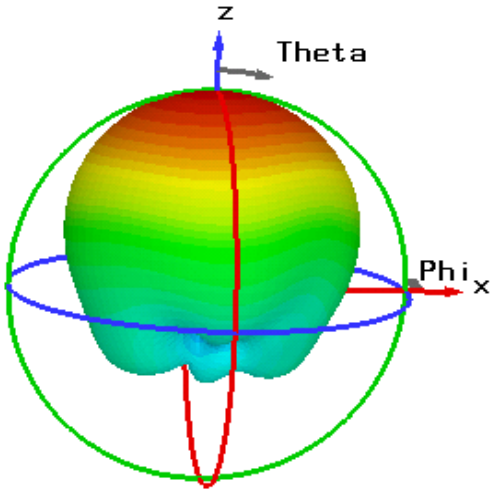

FIGURE 2.4: 3D RADIATION PATTERN OF A CIRCULAR PATCH ANTENNA

For a microstrip antenna, the E-plane pattern is normally broader than the H-plane patterns. And both patterns present distortions due to the truncation of the ground plane, which cause edge diffraction.

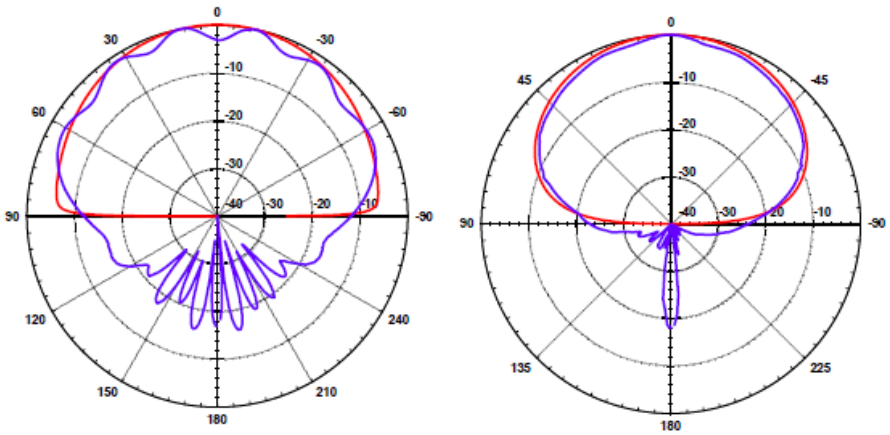

FIGURE 2.5: E-PLANE AND H-PLANE RADIATION PATTER. THE RED LINE CORRESPOND TO A RADIATION PATTERN WITH INFINITE SUBSTRATE AND GROUND PLANE, AND THE BLUE LINE CORRESPOND TO A RADIATION PATTERN WITH 1 METER GROUND PLANE

DIRECTIVITY AND GAIN

The directivity is a parameter related with the ability of the antenna to focus energy in a particular direction. It depends on the shape of the radiation pattern and it is always greater than one [24]. The equation to determine the directivity is as follows:

$$D = \frac{\frac{1}{2}\, Re\{E_\theta H_\phi^* - E_\phi H_\theta^*\}|_{\theta=0}}{\frac{P_r}{4\pi r^2}} = \frac{\frac{r}{2\eta_0}\left(|E_\theta|^2 + |E_\phi|^2\right)|_{\theta=0}}{\frac{P_r}{4\pi}} \tag{2.23}$$

where E_θ, H_θ, E_ϕ, H_ϕ are the radiation fields, P_r is the radiated power and η_0 is the wave impedance in free space $120\pi\ \Omega$.

Regarding to the gain, it can be defined as the directivity reduced by the losses of the antenna structure. The gain can be obtained multiplying the directivity by the efficiency of the antenna, e_r [19]:

$$G = e_r D \tag{2.24}$$

BANDWIDTH

Bandwidth is the range of usable frequencies within which the performance of the antenna, with respect to some characteristics conforming to a specified standard [25].

In microstrip antennas, the bandwidth is directly proportional to the substrate thickness and inverse proportional to the permittivity of the substrate. Since the substrates are usually thin, microstrip antennas have a narrow bandwidth [26].

For narrow antennas the bandwidth can be calculated as:

$$BW = \frac{f_{max} - f_{min}}{f_0} \cdot 100 \tag{2.25}$$

And for broadband antennas the bandwidth can be specified by:

$$BW = \frac{f_{max}}{f_{min}} \tag{2.26}$$

where:

f_{max}: the maximum frequency that meets the specifications

f_{min}: minimum frequency that meets the specifications

f_0: frequency in the center

RETURN LOSS

Return loss or reflection loss is a term related with the effectiveness of the power delivery from a transmission line to an antenna. This term is also related with the impedance matching and the maximum transfer power theory [27]. In a two-port network, the return loss can be identified as the S_{11} parameter.

This parameter is defined as the incident power (P_{in}) over the reflected power (P_r). Expressed in dB, the return loss is:

$$RL = 10 \log \frac{P_{in}}{P_r} \tag{2.27}$$

For a good transmission, a high return loss is desirable.

2.4. MICROWAVE NETWORK CHARACTERIZATION

This section reviews two of the most important parameters used to characterize microwave networks, the S-parameters and the ABCD parameters. Section 2.4.1 reviews the basic theory of the S-parameters and their characteristics for different networks. Section 2.4.2 presents the basic theory for the ABCD parameters and their characteristics. Finally, Section 2.4.3 presents the equations used for the conversion between the S-parameters and the ABCD parameters.

2.4.1. SCATTER PARAMETERS

Scatter Parameters, also called S-parameters, model the relationship between the transmitted and the incident power of a group of incident waves in one device. Furthermore, these parameters are related to the voltage and the current in the device port, they are frequency dependent and they are useful to characterize lineal active and passive devices [14].

These parameters are important in microwave design because they are the easiest tool to measure and work with at high frequencies. These parameters can be determined using network analysis techniques or a vector analyser (VNA).

All the S-parameters can be written in a matrix, called scattering matrix which provides a complete description of the network.

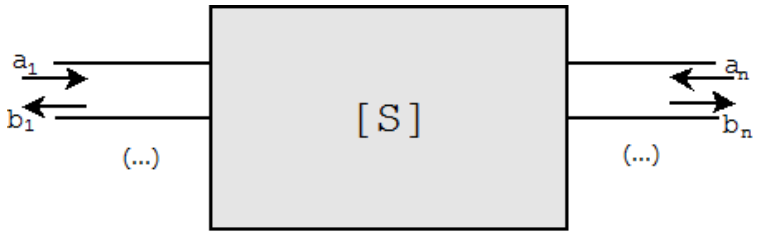

FIGURE 2.6: N PORTS DEVICE

For a device like the one of (Fig. 2.6), where a_n is the incident wave and b_n is the reflected wave in the n port, the relationship between these two waves is characterized by the S-parameters [S] of the device using the following matrix product [16]:

$$B = [S] \cdot A \quad \rightarrow \quad \begin{bmatrix} b_1 \\ b_2 \\ \vdots \\ b_n \end{bmatrix} = \begin{bmatrix} s_{11} s_{12} \dots s_{1n} \\ s_{21} s_{22} \dots s_{2n} \\ \vdots \quad \vdots \quad \ddots \quad \vdots \\ s_{n1} s_{n2} \cdots s_{nn} \end{bmatrix} \begin{bmatrix} a_1 \\ a_2 \\ \vdots \\ a_n \end{bmatrix} \tag{2.28}$$

The development of this equation could be simplified doing the analysis for a specific device, the quadripole also called two-port network, which can be seen in (Fig. 2.7). The two-port matrix is the most common scattering matrix, and this is the one that is going to be used in the experimental part. The two-port network will be completely defined by its S-parameters, S_{11}, S_{12}, S_{21} and S_{22}.

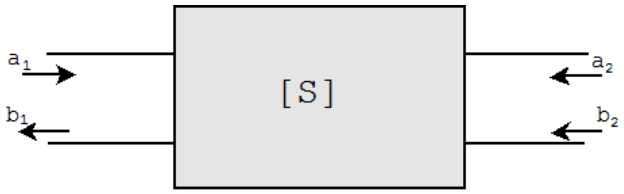

FIGURE 2.7: TWO-PORT ELEMENT OR NETWORK

$$\begin{bmatrix} b_1 \\ b_2 \end{bmatrix} = \begin{bmatrix} s_{11} & s_{12} \\ s_{21} & s_{22} \end{bmatrix} \begin{bmatrix} a_1 \\ a_2 \end{bmatrix} \tag{2.29}$$

$$S_{11} = \frac{b_1}{a_1}\Big|_{a_2=0} \quad S_{12} = \frac{b_1}{a_2}\Big|_{a_1=0} \quad S_{21} = \frac{b_2}{a_1}\Big|_{a_2=0} \quad S_{22} = \frac{b_2}{a_2}\Big|_{a_1=0} \tag{2.30}$$

where S_{11} is the reflexion coeficient looking into first port and S_{21} is the transmission coeficient from second port to first port.

These S_{11} and S_{21} are determined by measuring the amplitude and the phase of the incident, reflected and transmitted signals when the output is terminated in a matched load so a_2 is 0. Likewise, by placing the source at port 2 and terminating port 1 in a matched load, it is possible to obtain S_{12} and S_{22}. S_{22} is the reflection coeficient for second port and S_{12} is the transmission coeficient from first port to second port.

From these particular results of the two-port network, it is easy to extrapolate the results for a N ports device. A specific element of this generalized scattering matrix could be seen in the following equation:

$$S_{ij} = \left.\frac{b_i}{a_j}\right|_{a_k=0 \; for \; k \neq j} \tag{2.31}$$

In (Eq. 2.31), S_{ij} is the transmission coefficient from port i to port j when all other ports are terminated in matched loads. For i=j the S-parameter, S_{ii}, is the reflexion coefficient in the i^{th} port when all the other ports are terminated in matched loads.

S-PARAMETERS CHARACTERISTICS

For different kinds of components or networks, the S-parameters present different useful properties [28].

In the case of a reciprocal n-port network, normally made of different passive components, the S-matrix present the relation $S_{ij}=S_{ji}$ for all i and j. If the n-port network is passive and lossless, the S-matrix is unitary, so in this case the S-matrix satisfies the relation $([S]^*)^T \cdot [S]=1$.

In the specific case of a two-port network, it is symmetric when it is reciprocal ($S_{21}=S_{12}$) and when the output reflection coefficient are equal ($S_{11}=S_{22}$). In this specific case, if the network is passive and lossless,

$$|S_{11}| = |S_{21}| \quad |S_{22}| = |S_{12}| \tag{2.32}$$

2.4.2. ABCD MATRIX

To characterize a microwave network with an arbitrary number of ports the S-parameters described in Section 2.4.1. can be used. However, many microwave networks consist of a cascade of two-port networks. For this reason is easier to use an ABCD matrix.

The ABCD matrix is a 2x2 transmission matrix, and can be defined as:

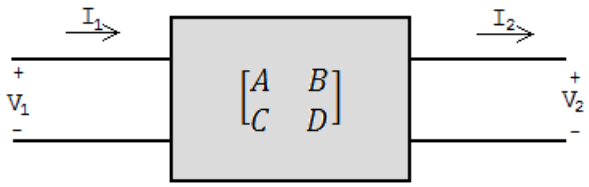

FIGURE 2.8: TWO-PORT NETWORK

$$\begin{bmatrix} V_1 \\ V_2 \end{bmatrix} = \begin{bmatrix} A & B \\ C & D \end{bmatrix} \begin{bmatrix} I_1 \\ I_2 \end{bmatrix} \tag{2.33}$$

where V are the voltages and I are the currents as show in the (Fig. 2.8).

This matrix is very useful to study the elements from a microwave network because each ABCD matrix can define one two-port element. The multiplication of the different ABCD matrixes of each network element, determines the ABCD matrix of the two-port network [14].

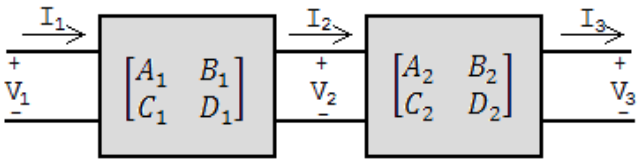

FIGURE 2.9: TWO-PORT ELEMENTS IN CASCADE

$$\begin{bmatrix} A & B \\ C & D \end{bmatrix} = \begin{bmatrix} A_1 & B_1 \\ C_1 & D_1 \end{bmatrix} \begin{bmatrix} A_2 & B_2 \\ C_2 & D_2 \end{bmatrix} \tag{2.34}$$

ABCD PARAMETERS PROPERTIES

As the S-parameters, the ABCD parameters have relevant properties for different kinds of networks [14].

For a reciprocal network, the ABCD parameters have to satisfy the relationship:

$$AD - BC = 1 \tag{2.35}$$

Furthermore, if the network is lossless, A and D have to be real and B and C imaginary.

2.4.3. S-PARAMETERS TO ABCD PARAMETERS CONVERSION

The S-parameters for a two-port network are related with the ABCD parameters by the following conversion equations [14].

$$\begin{aligned} S_{11} &= \frac{A + \frac{B}{Z_0} - CZ_0 - D}{A + \frac{B}{Z_0} + CZ_0 + D} \qquad S_{12} = \frac{2(AD - BC)}{A + \frac{B}{Z_0} + CZ_0 + D} \\ S_{21} &= \frac{2}{A + \frac{B}{Z_0} + CZ_0 + D} \qquad S_{22} = \frac{-A + \frac{B}{Z_0} - CZ_0 + D}{A + \frac{B}{Z_0} + CZ_0 + D} \end{aligned} \tag{2.36}$$

$$\begin{aligned} A &= \frac{(1 + S_{11})(1 - S_{22}) + S_{12}S_{21}}{2S_{21}} \qquad B = \frac{(1 + S_{11})(1 + S_{22}) - S_{12}S_{21}}{2S_{21}} Z_0 \\ C &= \frac{1}{Z_0}\frac{(1 - S_{11})(1 - S_{22}) - S_{12}S_{21}}{2S_{21}} \qquad D = \frac{(1 - S_{11})(1 + S_{22}) + S_{12}S_{21}}{2S_{21}} \end{aligned} \tag{2.37}$$

with Z_0 being the characteristic impedance.

2.5. POST PROCESSING METHODS

This section presents the two post processing techniques that are going to be used in the experimental part. These two techniques are the Thru, Reflect and Line calibration in free space (Section 2.51) and the Nicolson Ross Weir method (Section 2.5.2).

2.5.1. THRU REFLECT LINE CALIBRATION IN FREE SPACE

The Thru-Reflect-Line (TRL) technique in free space is a modification of the calibration technique used for the Vector Network Analyzer (VNA). This calibration is used to remove systematic errors from the S-parameters caused by transmission losses or mismatches of the antennas [29].

TRL calibration is a full two-port calibration method that uses three different connexions: Thru, Reflect and Line. The TRL free space calibration is based on the same process as the normal TRL calibration, but with a few modifications. This TRL calibration in free space is oriented to the assemblies that use antennas. For the TRL calibration in free space, the Thru connection is made by connecting the two antennas with an air gap in between. This air gap corresponds to two times the focal length of the antennas. The Reflect connection uses a perfect electric conductor (PEC) as a load placed between the two antennas. And, the Line connection is made by adding an extra air gap between the antennas. The length of this extra gap corresponds to $\lambda/4$ where λ is the wavelength in the middle of the operation range [30]. These three connexions are employed to obtain the scattering parameters of an error box.

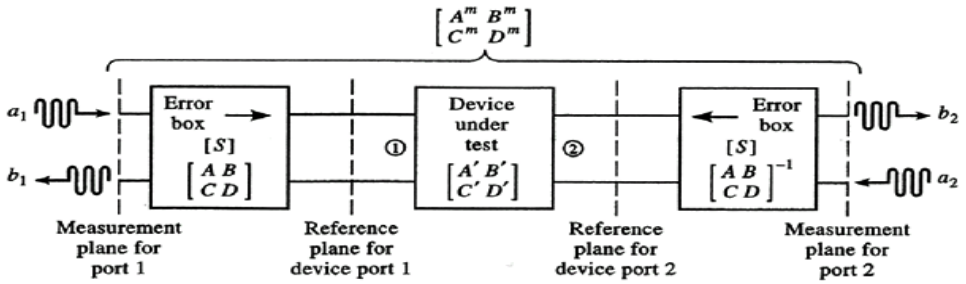

FIGURE 2.10: MATHEMATICAL MODEL OF THE TRL CALIBRATION [14]

During the analytical development to obtain the error box, the Thru S-matrix is going to be denote as [T], the Reflection S-matrix is going to be denoted as [R] and the Line S-matrix is going to be denoted as [L]. Moreover, to add simplicity to the analytical calculations, it is going to be assumed that ports 1 and 2 have the same characteristic impedance and that the error box is reciprocal (S_{12}=S_{21}) and identical for both ports [14].

The Thru S-parameters can be related with the error box S-parameters as follows:

$$T_{11} = S_{11} + \frac{S_{21}S_{12}^2}{1 - {S_{22}}^2} \qquad T_{12} = \frac{S_{12}^2}{1 - {S_{22}}^2} \tag{2.38}$$

Using the symmetry and reciprocity of the system, T_{11}=T_{22} and T_{12}=T_{21}.

For the Reflect connexion:

$$R_{11} = S_{11} + \frac{S_{12}^2\Gamma_L}{1 - S_{22}\Gamma_L} = R_{22} \qquad R_{21} = 0 = R_{12} \tag{2.39}$$

where Γ_L is the reflection coefficient of the conductor placed between the waveguides in the Reflect connexion.

Finally, for the Line connexion:

$$L_{11} = S_{11} + \frac{S_{22}S_{12}^2 e^{-2\gamma l}}{1 - {S_{22}}^2 e^{-2\gamma l}} = L_{22} \qquad L_{12} = \frac{S_{12}^2 e^{-\gamma l}}{1 - {S_{22}}^2 e^{-2\gamma l}} = L_{21} \tag{2.40}$$

Using the equations (Eq. 2.38, 239 and 2.40) is possible to determine the values of the S-parameters of the error box, $e^{-\gamma l}$ and Γ_L. The full analytic development to find the solutions to these five unknowns is detailed in [14].

$$e^{-\gamma l} = \frac{L_{12}^2 + T_{12}^2 - (T_{11} - L_{11})^2 \pm \sqrt{[L_{12}^2 + T_{12}^2 - (T_{11} - L_{11})^2]^2 - 4L_{12}^2 T_{12}^2}}{2L_{12}T_{12}} \tag{2.41}$$

This equation (Eq. 2.41) present two possible solutions. To decide which one is the correct solution; the criterion of [14] has been used. This criterion is based in the requirement that the real and imaginary parts of the propagation constant (γ) have to be positive.

$$S_{22} = \frac{T_{11} - L_{11}}{T_{12} - L_{12}e^{-\gamma l}} \tag{2.42}$$

$$S_{11} = T_{11} - S_{22}T_{12} \tag{2.43}$$

$$S_{12}^2 = T_{12}(1 - S_{22}^2) \tag{2.44}$$

$$\Gamma_L = \frac{R_{11} - S_{11}}{S_{12}^2 + S_{22}(R_{11} - S_{11})} \tag{2.45}$$

After solving these equations, it is easy to obtain the ABCD parameters of the error box. And then, the S-parameters of the device under test (DUT) can be obtained from the measured S-parameters. To obtain the DUT parameters, it is simple to operate with the ABCD matrix because the system is a two-port system. The resulting ABCD parameters of the DUT are:

$$\begin{bmatrix} A' & B' \\ C' & D' \end{bmatrix} = \begin{bmatrix} A & B \\ C & D \end{bmatrix}^{-1} \begin{bmatrix} A_m & B_m \\ C_m & D_m \end{bmatrix} \begin{bmatrix} A & B \\ C & D \end{bmatrix} \tag{2.46}$$

Knowing the ABCD is easy to obtain the S-parameter of the DUT using the equations (Eq. 2.36).

After the application of this calibration, the reference planes are located in the DUT, and the S-parameters are free of undesirable effects. Therefore, the Nicolson Ross Weir (NRW) can be applied.

2.5.2. NICOLSON ROSS WEIR METHOD

Nicolson Ross Weir is a methodology used to obtain the permittivity and the permeability from the S-parameters. This method combines the values of S_{11} and S_{21} to develop an equation system that allows the estimation of the complex electromagnetic constants. The NRW method works well for frequencies away from the TEM mode. Near resonance, however, the method loses sensitivity for low-loss materials [31].

This method obtains the permittivity and permeability using the following constants [32][33].

$$K = \frac{S_{11}^2 - S_{21}^2 + 1}{2S_{11}^2} \tag{2.47}$$

Using the constant K of the (Eq. 2.47) is possible to obtain the reflection and transmission coefficients, Γ and T respectively.

$$\Gamma = K \pm \sqrt{K^2 - 1} \qquad T = \frac{S_{11} + S_{21} - \Gamma}{1 - (S_{11} + S_{21})\Gamma} K = \frac{S_{11}^2 - S_{21}^2 + 1}{2S_{11}^2} \tag{2.48) (2.49}$$

After the calculation of the reflection and transmission coefficients and knowing that the propagation constant has to be $|\Gamma| \leq 1$, is possible to obtain the values of the permittivity (ε*) and the permeability (μ*).

$$\gamma = \frac{\ln(1/T)}{d} \qquad \gamma_0 = j\frac{2\pi}{\lambda_0} \tag{2.50}$$

$$\varepsilon^* = \frac{\gamma}{\gamma_0}\left(\frac{1-\Gamma}{1+\Gamma}\right) \qquad \mu^* = \frac{\gamma}{\gamma_0}\left(\frac{1+\Gamma}{1-\Gamma}\right) \tag{2.51) (2.52}$$

3. WAVEGUIDE STRUCTURE EXPERIMENTS

This chapter presents the different results of the waveguide structure simulations. Section 3.1, will present the goal of the experiment. Then, the Section 3.2 will present the properties of the assembly and the simulation parameters. Finally, Section 3.3 will show the different results obtained from the simulations and the post processing part.

3.1. INTRODUCTION

The waveguide structure is the first setup under study. It consists of two waveguides with an acrylic tank in between, and other support components.

The objective is to run a simulation of this assembly using CST software to determine the S-parameters of the sample placed inside the tank. After the simulation, the aim is to compare the obtained parameters with the experimental ones and extract the permittivity and permeability of different glucose solutions. These experimental results came from an experiment did by MediWiSe before my enrolment in the project.

3.2. SIMULATION SETUP

3.2.1. SIMULATION ASSEMBLY

The simulation assembly is a replication of the assembly used in the experimental part by MediWiSe.

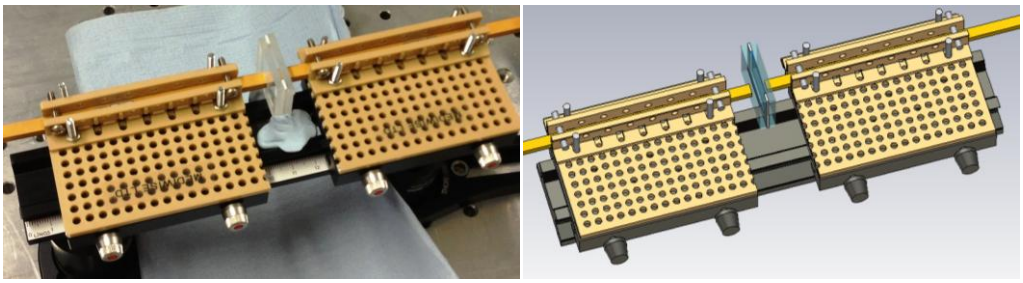

FIGURE 3.1: LEFT FIGURE CORRESPOND TO THE EXPERIMENTAL ASSEMBLY AND THE RIGHT FIGURE CORRESPOND TO THE SIMULATION ASSEMBLY IN CST

This assembly includes seven different parts: the rail, the rail carriers, the grid, the waveguide support, the waveguides, the tank and the bolts. The rail (40 mm x 15 mm x 200mm), the rail carrier (59.8 mm x 12.5 mm x 80 mm) and the bolts are metals and are therefore considered to be perfect electric conductors (PECs). The grid (60 mm x 3 mm x 80 mm) and the waveguide support (22 mm x 11 mm x 80 mm) are made of plastic with $\varepsilon=2$ and $\mu=1$. The waveguides are rectangular with 2.8796 mm x 4.7592 mm x 118.5 mm external dimensions and 0.5 mm of thick. These waveguides are made of cooper material with $\sigma=5.8\cdot10^{7}$ S/m and $\mu=1$. The tank (30 mm x 24 mm x 7 mm) consists of three different slabs of material, the outside material is acrylic (2 slabs of 3 mm each one) with $\varepsilon=2.53$ $\tan\delta=0.0119$ at 60 GHz, and the middle material (1 mm slab) is styrene ($\varepsilon=2.725$ $\tan\delta=0.008$ at 60 GHz) [34].

The assembly presented above (Fig. 3.1) is the full assembly of the waveguide structure. However, some experiments have been done using a simplified model of this experiment in order to save simulation time. This simplified model consists of two waveguides separated by 7 mm, and 1 mm acrylic slab between them. This 8 mm gap between the waveguides has been used in order to approximate the transmission waves as a plane waves.

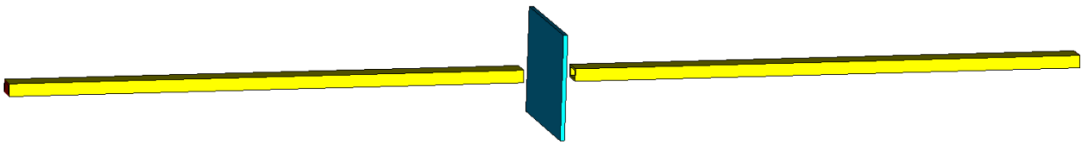

FIGURE 3.2: SIMPLIFIED ASSEMBLY

3.2.2. SIMULATION PARAMETERS

The simulation parameters must be defined correctly in order to model the true experimental process accurately and obtain the corresponding results. A ist of the parameters used in the simulation process is given below.

- Set units: all the simulations use mm as unit for dimension and GHz as the frequency unit.

- Background material: the background material for all the simulations is air ($\varepsilon_r=1$ and $\mu_r=1$).

- Excitation: to calculate the S-matrix of the structure, different excitation ports need to be defined. For all our simulations, waveguide ports will be used as excitation because they

offer a better match to the mode pattern as well as higher accuracy in S-Parameters. These ports are going to be located in the external edges of the waveguides.

- Boundary conditions: these are necessary because the computers are only capable of calculating problems with finite dimensions. For all the simulations the boundary conditions are open space.

- Mesh density: the mesh density is related to the resolution of the simulation. The values of this parameter are different for each simulation in order to get the best results for each simulation. In the simulations with waveguide structure, the meshcells are between 10 million and 100 million.

- Frequency range: to simulate this structure the frequency range is set between 50 GHz and 75 GHz (V-band).

3.3. SIMULATION RESULTS AND DISCUSSION

3.3.1. FIELDS DISTRIBUTION

This section will present the distributions of the electric field, the magnetic field and the power flow in the waveguide structure. These simulation results have been obtained using the full assembly with the tank filled with 3% glucose solution. To obtain the fields, different monitor fields at 60 GHz have been added to the simulation options. For the magnetic and electric fields, these monitor fields store the electric and magnetic fields vectors and plot them. For the power flow, the computer stores the Poynting vector of the electromagnetic field and represents the maximum value (peak value) of the power flow at every spatial point, encountered within one period of time.

For the waveguide structure (Fig. 3.1) the electric field only presents E_y component inside the waveguide, the other two components, E_x and E_z are zero.

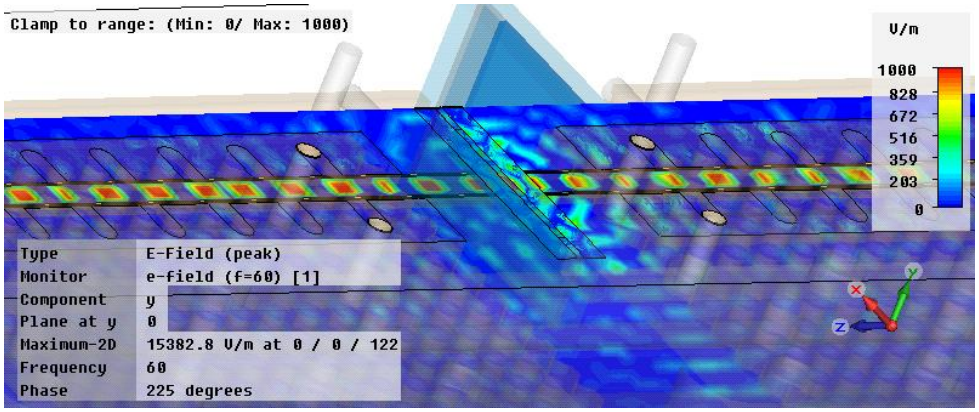

FIGURE 3.3: E_Y DISTRIBUTION.

Regarding to the magnetic field, the structure only presents magnetic field for the H_x and H_z components. The H_y component is zero.

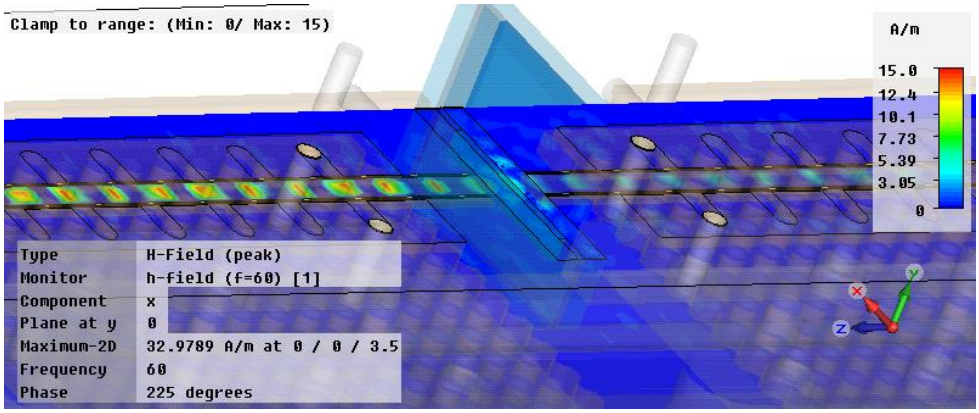

FIGURE 3.4: H_X DISTRIBUTION

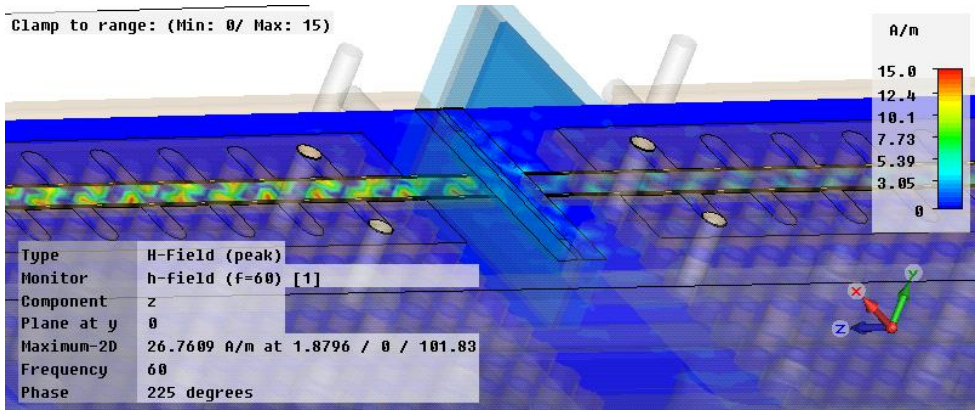

FIGURE 3.5: H_Z DISTRIBUTION

After the representation of the magnetic and the electric fields, is possible to guess the operating mode of the waveguide. In this case the waveguide mode is a TE mode because E_z is zero. Furthermore, the operation mode of the waveguide cannot be TM mode because H_z is not zero.

Finally, the representation of the absolute power flow distribution is as follows.

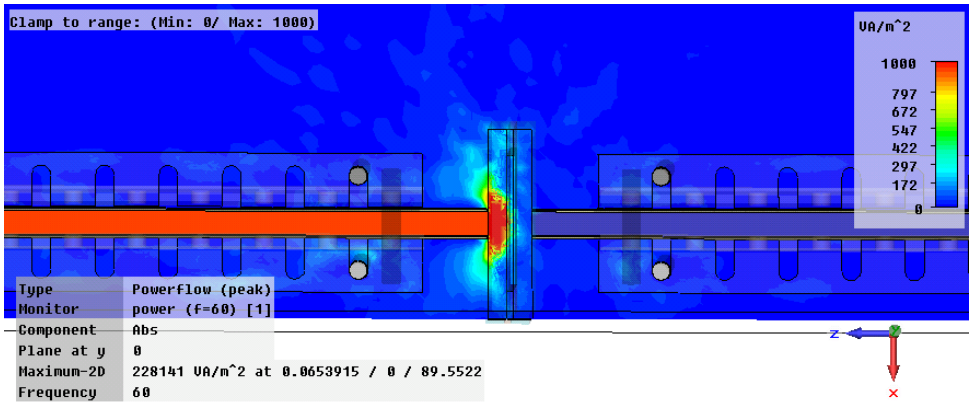

FIGURE 3.6: POWERFLOW ABSOLUTE DISTRIBUTION

From (Fig. 3.6), it can be noticed that the power is absorbed by the glucoses concentration. However, if the experiment uses an empty tank, the power passes thru the tank and arrives to the second port (Fig. 3.7).

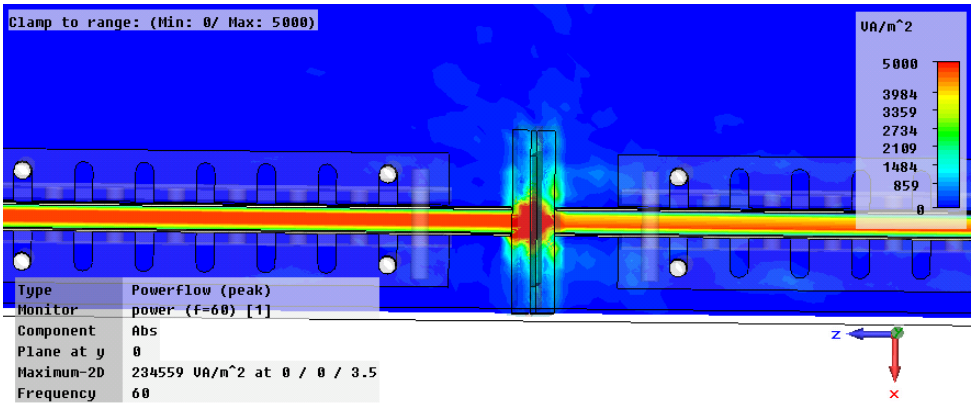

FIGURE 3.7: POWERFLOW ABSOLUTE DISTRIBUTION FOR AN ASSEMBLY WITH AN EMPTY TANK

3.3.2. S-PARAMETERS FOR DIFFERENT GLUCOSE CONCENTRATIONS

This section presents the results for four different solutions inside the tank, air, distilled water, 0.5% glucose concentration in water and 3% glucose concentration in water. The aim of this experiment is compare the experimental results obtained by MediWiSe with the CST simulation results.

The glucose solutions used in the simulation have the dielectric dispersions found in [35].

	Distilled water	0.5% glucose	3% glucose
9.3 GHz	60.7+ j34	60.4+j33.8	58.3+j32.9
28.1 GHz	24.3+j31.5	23.8+j30.7	23.0+j30.2
31.3 GHz	21.8+j31	21.8+j30.1	21.8+j29.4
37.0 GHz	18.4+j27.8	18.1+j27.2	16.2+j26.3
42.7 GHz	14.6+j24.8	14.4+j21.6	14.0+j23.7
48.1 GHz	14.5+j24.8	14.4+j24.5	14.0+j23.7
62.6 GHz	10.8+j18.9	10.7+j18.6	10.4+j17.9
77.4 GHz	8.63+j15.21	8.53+j15.15	8.28+j14.58
83.5 GHz	8.29+j14.02	8.19+j13.91	7.6+j13.39
92.7 GHz	7.78+j13.13	7.76+j13.05	7.55+j13.32

TABLE 3.1: COMPLEX PERMITTIVITY FOR DIFFERENT FREQUENCIES AND GLUCOSE CONCENTRATIONS

The comparison between them and the experimental results can be found in the following figures.

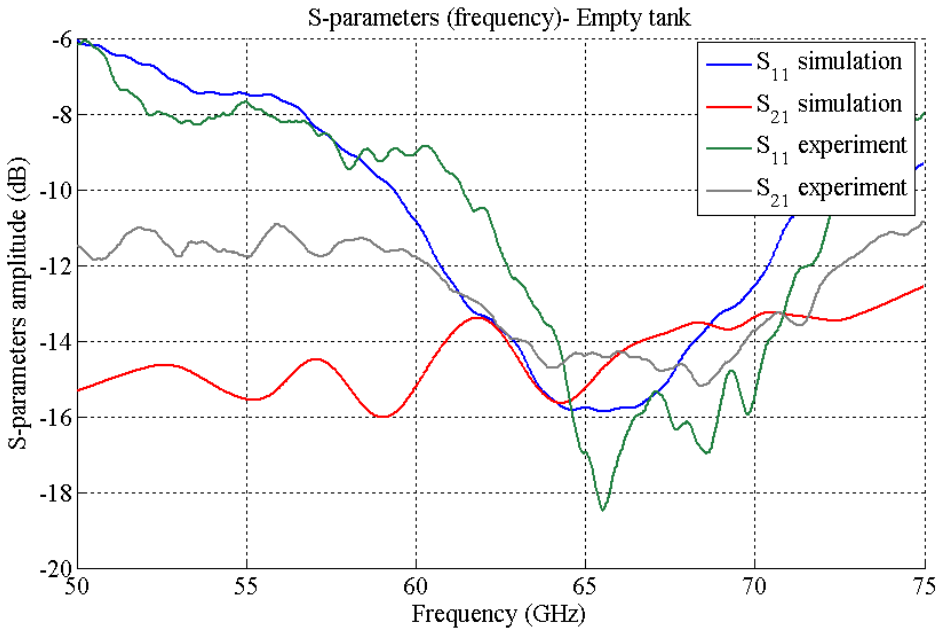

FIGURE 3.8: S-PARAMETERS AGAINST THE FREQUENCY FOR AN EMPTY TANK

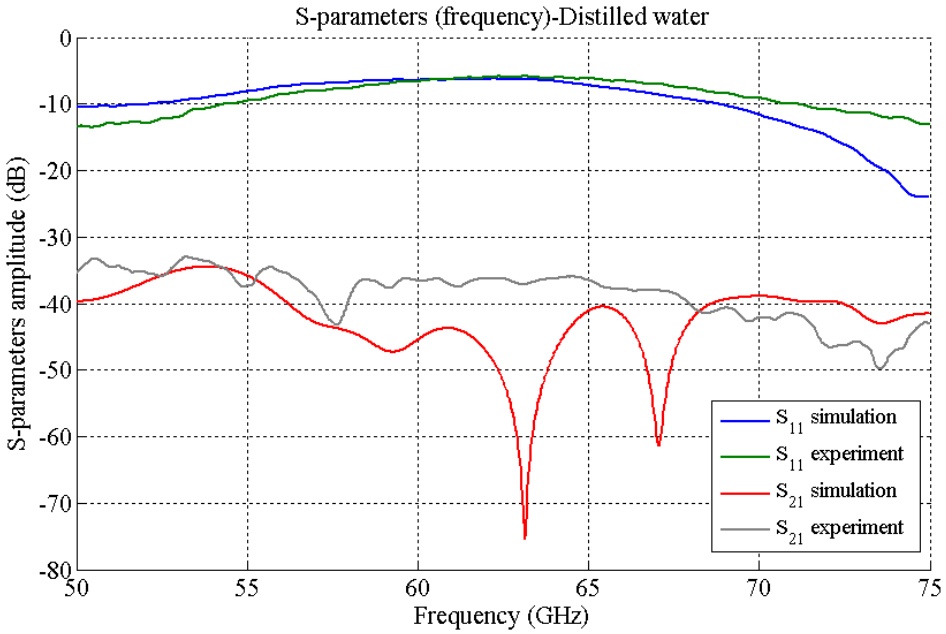

FIGURE 3.9: S-PARAMETERS AGAINST THE FREQUENCY FOR DISTILLED WATER SOLUTION INSIDE THE TANK

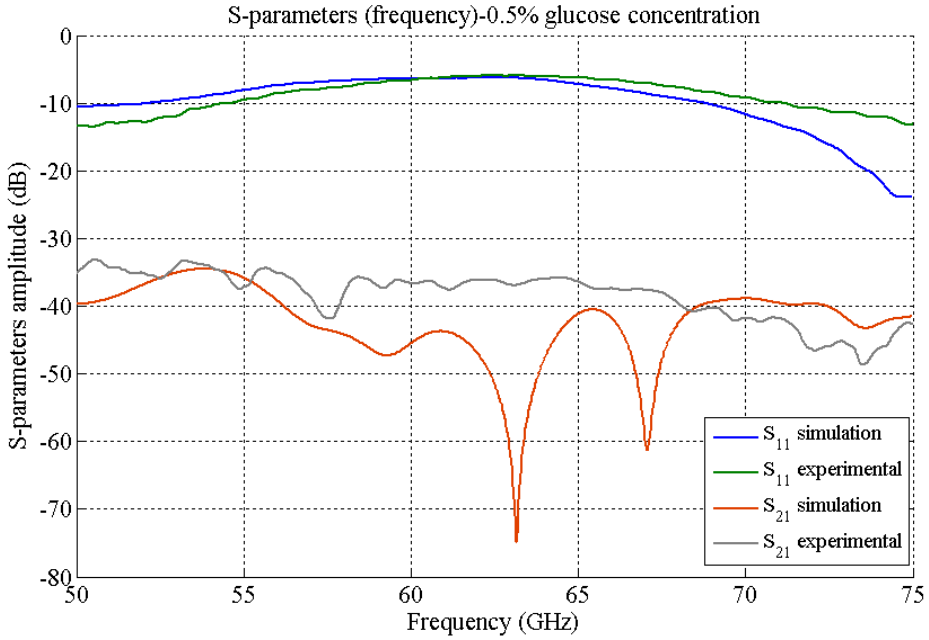

FIGURE 3.10: S-PARAMETERS AGAINST THE FREQUENCY FOR 0.5% GLUCOSE SOLUTION INSIDE THE TANK

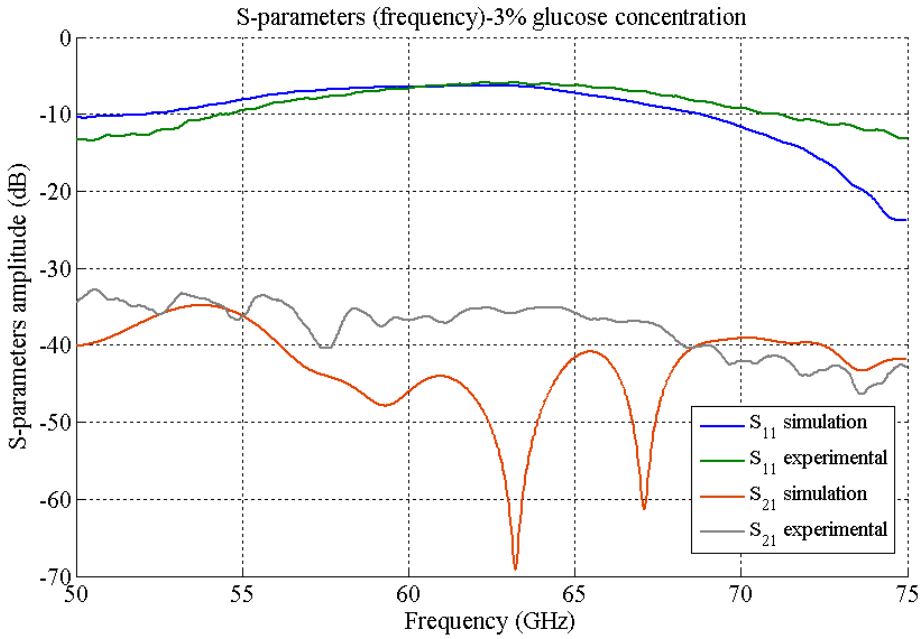

FIGURE 3.11: S-PARAMETERS AGAINST THE FREQUENCY FOR 3% GLUCOSE SOLUTION INSIDE THE TANK

After the simulations, the values of the S-parameters for the different solutions at 60 can be found in the following table:

Solution	Experimental S_{11}	Simulation S_{11}	Experimental S_{21}	Simulation S_{21}
Air	-9.034 dB (0.3534)	-10.84 dB (0.2871)	-11.79 dB (0.2573)	-15.2 dB (0.1738)
Distilled water	-6.648 dB (0.4651)	-6.417 dB (0.4778)	-36.55 dB (0.01488)	-45.43 dB ($5.352 \cdot 10^{-3}$)
0.5% Glucose concentration	-6.661 dB (0.4645)	-6.426 dB (0.4772)	-36.76 dB (0.01452)	-46.04 dB ($4.989 \cdot 10^{-3}$)
3% Glucose concentration	-6.692 dB (0.4628)	-6.463 dB (0.4752)	-36.62 dB (0.01476)	-45.48 dB ($5.321 \cdot 10^{-3}$)

TABLE 3.2: S-PARAMETERS AMPLITUDE AT 60 GHZ FOR DIFFERENT SOLUTIONS (ABSOLUTE VALUES AND dB)

From figures (Figs. 3.9, 3.10, 3.11), it can be noticed that all the results for the different glucose concentrations are very similar. This fact suggests that the amount of glucose in water is not sufficient to make big changes in the S-parameters. Nevertheless, it is possible to notice a small difference between them. This small difference determines the necessary sensitivity to detect the changes in glucose concentration. From the table (Table 3.2) is possible to establish that this sensitivity is of the order of ±0.01 dB.

The comparison between the simulation results and the experimental results shows that the simulated values for S_{11} are more similar to the experimental values than the S_{21} parameters, especially in the range 58 GHz - 65GHz, see (Figs. 3.9, 3.10, 3.11). The simulated S_{11} is very similar to the experimental results.

Regarding to S_{21}, it can be seen from the figures (Figs. 3.9, 3.10, 3.11) that the results are not as similar as the S_{11} result. Notably, resonance peaks in S_{21} values are observed only for the simulation results.

3.3.3. TRL CALIBRATION AND NRW METHOD

The aim of this experiment is to obtain the permittivity and permeability of a solution placed inside the tank using the TRL calibration to remove the undesirable effects of the assembly and the NRW method to extract the permittivity and permeability from the S-parameters after the calibration.

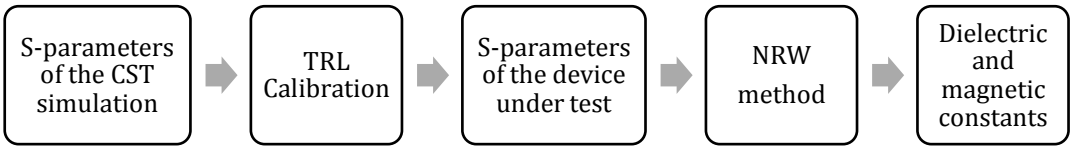

FIGURE 3.12: SCHEME OF THE EXPERIMENT STEPS

In this experiment, the assembly used to test this method is the simplified model explained in Section 3.2.1 (Fig. 3.2). For this experiment a slab of homogenous material has been used because the NRW method only works for homogeneous mediums [32][33]. Moreover this simplified model helps to save simulation time.

The theory of the TRL calibration in free space, explained in Section 2.5.1, says that the TRL calibration in free space is specific for antennas. However, in this experiment this calibration is adapted to work with a waveguide structure. For this reason, the calibration distances for the Thru and the Line have been adapted to this specific structure.

In this experiment, the distance between waveguides is set to 8 mm because at this distance the waves are more similar to plane waves. Therefore for the Thru the distance between waveguides is the 7 mm and for the Line is 8.25 mm because $\lambda/4$ is 1.25 mm.

To make the decision between the positive or the negative sing in (Eq. 2.41) the criterion based in the requirement that the real and imaginary parts of the propagation constant (γ) have to be positive has been applied. However, there are some frequencies that do not satisfy this criterion. For this reason, another less restrictive criterion has been used for these frequencies. This less restrictive criterion adds another condition to the previous one. This condition is met if the real part of the propagation constant is greater than zero.

After the application of all the conditions explained above, the calibration has been done and the results are as follows:

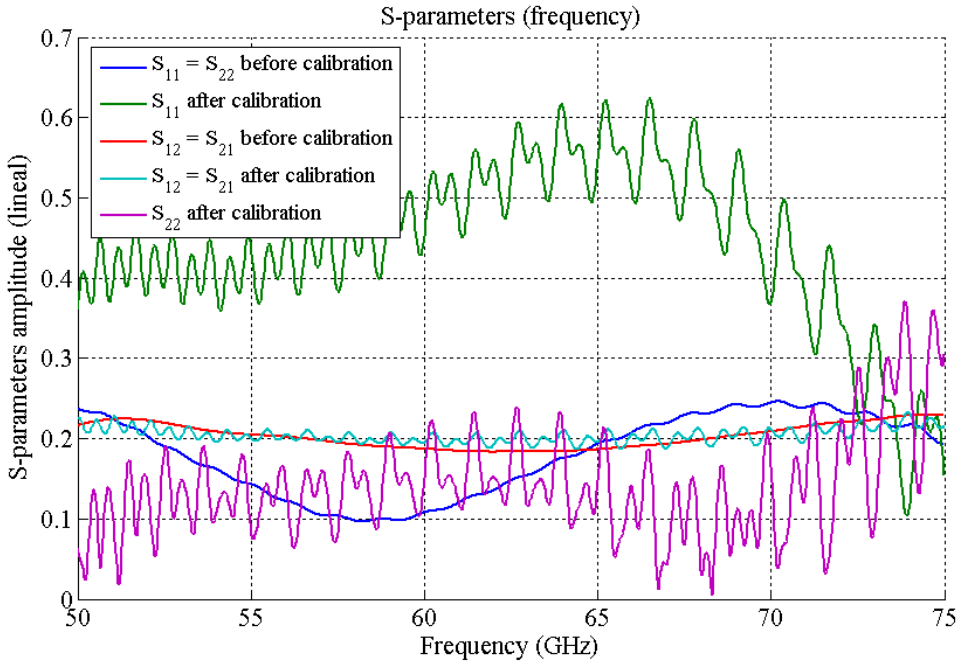

FIGURE 3.13: S-PARAMETERS AGAINST THE FREQUENCY BEFORE AND AFTER CALIBRATION

The figure above (Fig. 3.13) shows the S-parameters before and after calibration. However, there is a better way to represent the S-parameters to know if the TRL calibration works or not. For this reason, these S-parameters obtained after calibration will be compared with the ideal parameters. To do the comparison, first, is necessary to obtain the ideal parameters. To obtain these ideal parameters, the NRW method has been applied in the inverse order, using the permittivity and permeability of the acrylic (ε=2.53 and μ=1) to obtain the S-parameters.

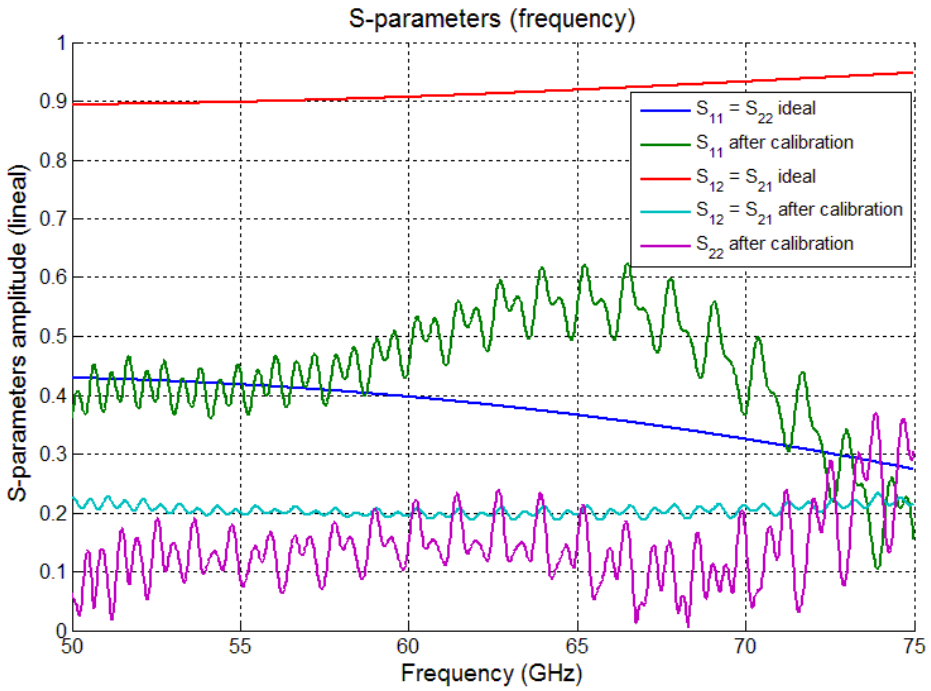

FIGURE 3.14: IDEAL AND AFTER CALIBRATION S-PARAMETERS AGAINST THE FREQUENCY

To obtain the dielectric constant, the NRW method has been applied. The comparison of this method with the ideal permittivity and permeability of the acrylic are showed in the next figure:

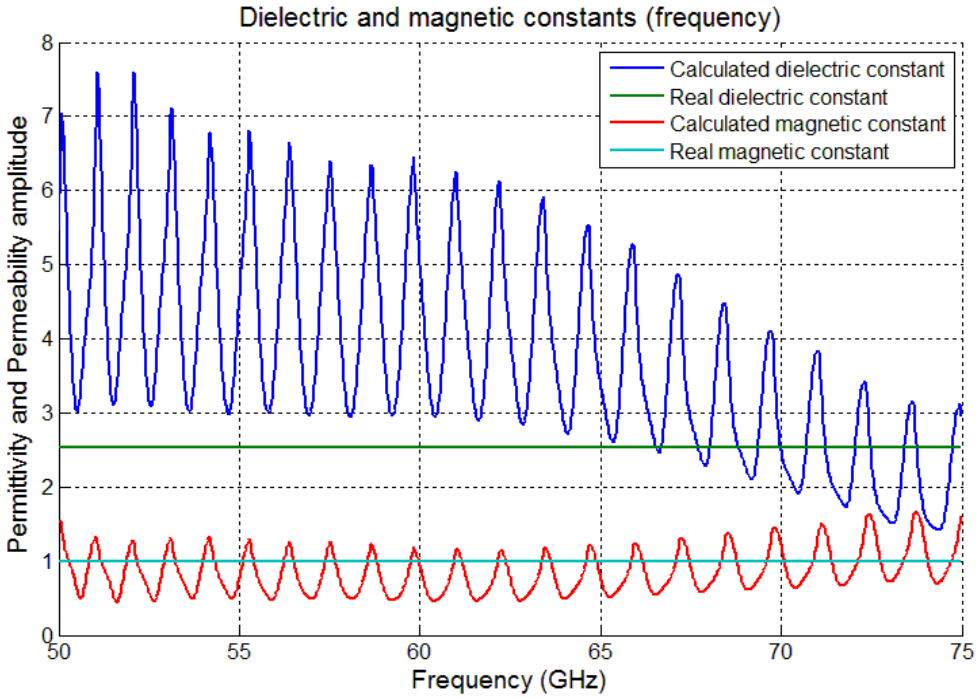

FIGURE 3.15: IDEAL AND CALCULATED (AFTER TRL AND NRW METHOD) PERMITTIVITY AND PERMEABILITY

From figures (Figs. 3.14, 3.15), it can be noticed that the calculated results (S-parameters after calibration and calculated permittivity and permeability) differ from the ideal parameters. This difference is due to the fact that our approximation to plane waves is not optimal. This fact is

because of the waveguides cannot produce perfect plane waves, which are required for the application of the NRW algorithm. For this reason, after some ideas that did not success, we decided to try to repeat the experiment using waveguides, specifically, using two circular patch antennas designed by MediWiSe for this glucose project.

4. ANTENNA STRUCTURE EXPERIMENTS

This chapter presents the various results from the antenna structure simulations. The first Section 4.1, describes the objectives of the experiment. Then, Section 4.2 will present the properties of the assembly and the simulation parameters. Finally, Section 4.3 presents the different results from the CST simulations and the post-processing part.

4.1. INTRODUCTION

Our antenna experimental setup consists of two microstrip antennas with an acrylic tank between them.

As in the waveguide experiments (Chapter 3), one of objectives is to run a simulation of this assembly using CST software to determine the S-parameters of the sample placed inside the tank, and then extract the permittivity and permeability of different glucose solutions using the resulting S-parameters from the simulation.

The other objective is to compare the sensitivity of this method with the sensitivity of the waveguide method to evaluate both methods.

4.2. SIMULATION SETUP

4.2.1. SIMULATION ASSEMBLY

The simulation assembly of the antenna structure consists of two patch antennas and the tank between them.

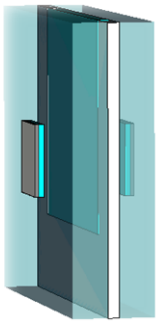

FIGURE 4.1: ANTENNA SIMULATION ASSEMBLY

Both antennas (6 mm x 6 mm x 0.802 mm) use proximity coupling feeding method and consist of different layers:

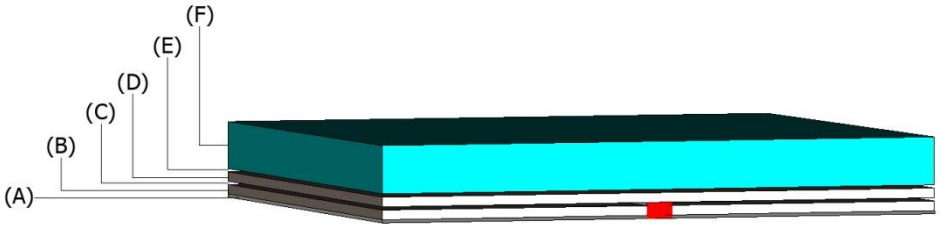

FIGURE 4.2: MICROSTRIP ANTENNA STRUCTURE

Flat parts	Thickness	Parameters
(A) Ground plane	34 μm	PEC
(B) Substrate: Rt5880	0.1 mm	ε = 2.2 and tanδ = 0.0009 at 10 GHz and μ = 1
(C) Microstrip line	34 μm	50 Ω
(D) Substrate: Rt5880	0.1 mm	ε = 2.2 and tanδ = 0.0009 at 10 GHz and μ = 1
(E) Circular patch	34 μm	Diameter: 1.6 mm
(F) Plastic cover: ABS	0.5 mm	ε=2.6

TABLE 4.1: CHARACTERISTICS OF THE DIFFERENT FLAT PARTS OF THE ANTENNA

The tank presented in (Fig. 4.1) has the same characteristics with the tank described in the waveguide chapter (Section 3.2.1).

4.2.2. SIMULATION PARAMETERS

The simulation parameters for this structure are defined before the simulation as follows.

- Set units: all the simulations use mm as unit for dimension and GHz as the frequency unit.

- Background material: the background material for all the simulations is air (ε_r=1 and μ_r=1). To get better results, the surrounding space in all the simulations for the antenna structure has been set to 5 mm.

- Excitation: different kind of ports have been tried to calculate the S-matrix of the antenna structure. The excitation that provided better results was waveguide ports, which were, therefore, chosen as the excitation type used in the simulations. These ports will be located in the bottom of the microstrip line and they are going to be connected with the ground plane. An example of the location of these ports can be found in (Fig. 4.2), where the port is the red part.

- Boundary conditions: all the simulations use an open space as a boundary condition.

- Mesh density: the values of this parameter are different for each simulation in order to get the best results for each simulation. These values are between (4 million meshcells and 130 million meshcells)

- Frequency range: for this structure, as for the waveguide structure, the frequency range is set between 50 GHz and 75 GHz.

4.3. SIMULATION RESULTS AND DISCUSSION

4.3.1. MICROSTRIP ANTENNA STUDY

The objective of this section is to study the properties of the antenna designed by MediWiSe.

The simulation assembly for this experiment consists of only one microstrip antenna, with physical characteristics described in Section 4.2.1.

In this experiment, two monitor fields at 60 GHz have been selected in the simulation options, the far field and the power flow monitors.

The far field monitor shows the radiation pattern of the antenna.

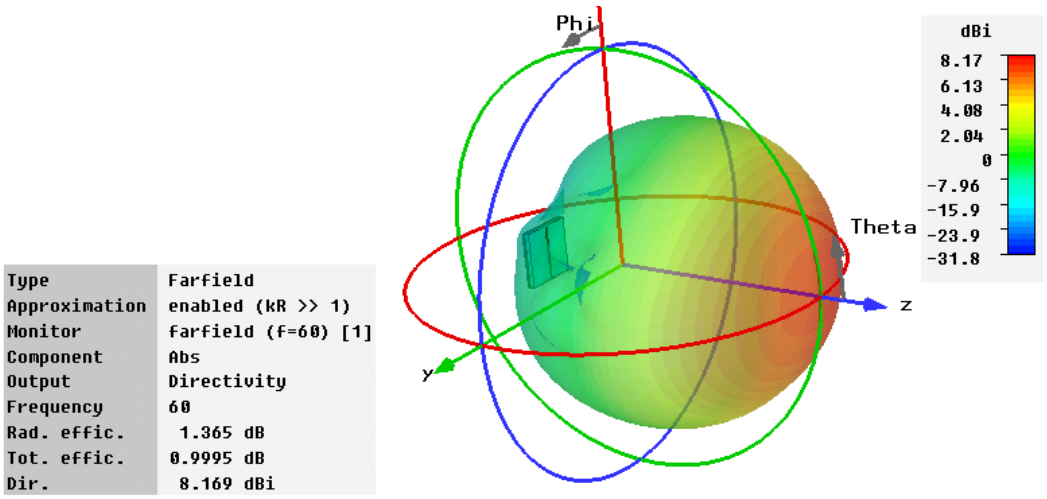

FIGURE 4.3: 3D RADIATION PATTERN OF THE MICROSTRIP ANTENNA AT 60 GHZ

Figure (Fig. 4.3) shows that the antenna radiates in the z positive direction since the highest directivity is concentrated in this direction. Furthermore, is possible to determine the directivity of the antenna. For our antenna, the maximum value of directivity is 8.169 dBi.

The power flow of the antenna is distributed in the z positive direction, as it can be seen in the following figure.

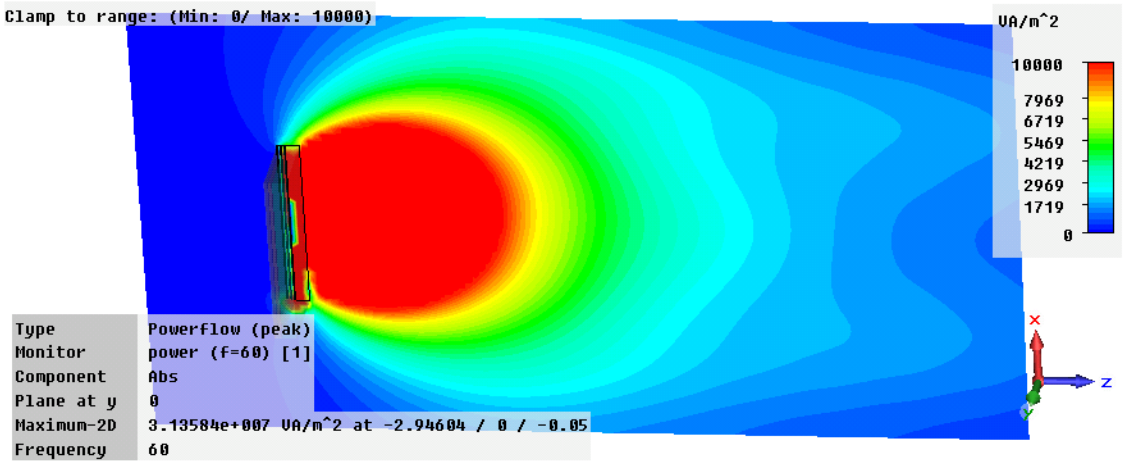

FIGURE 4.4: POWEFLOW DISTRIBUTION AT 60 GHZ

In this experiment, the return loss has been also studied. To study this antenna characteristic, S_{11} has been plotted to see the resonance frequency of the antenna.

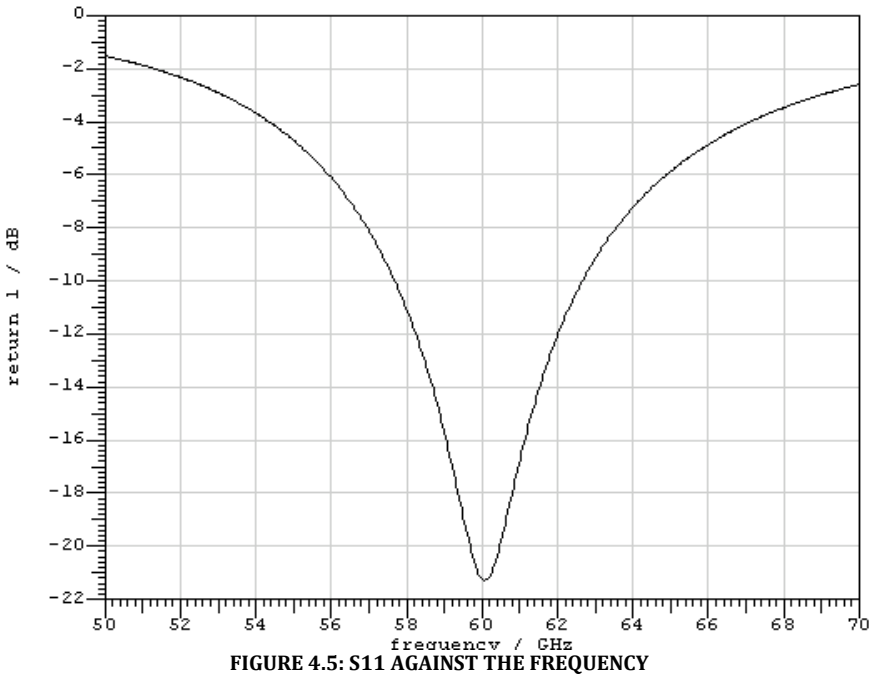

FIGURE 4.5: S11 AGAINST THE FREQUENCY

Figure (Fig. 4.5) shows that the antenna radiates best at around 60 GHz, where S_{11} is -21.3 dB. From this figure (Fig. 4.5) the bandwidth can be easily determined. This bandwidth can be defined as the frequency range where the value of S_{11} is under -10 dB. Therefore, the bandwidth would be between 57.7 GHz and 62.6 GHz, so this antenna has 4.9 GHz of bandwidth.

4.3.2. STUDY OF THE ANTENNA ASSEMBLY

The aim of this experiment is to study the behaviour of the complete antenna structure described in Section 4.2.1.

In this experiment the tank is filled with the same glucoses solutions used for the waveguide structure (Table 3.1). However, in this case, an interpolation of the glucose solution values between 48 GHz and 92.7 GHz have been done for all the glucose solutions. The objective of this interpolation is increase the number of values in the range of interest (45 GHz- 75 GHz) in order to obtain more accurate results. This interpolation is important because it helps to achieve better fitting between the curve of dielectric values and the curve that CST uses to simulate the results.

The power flow in this case is as follows:

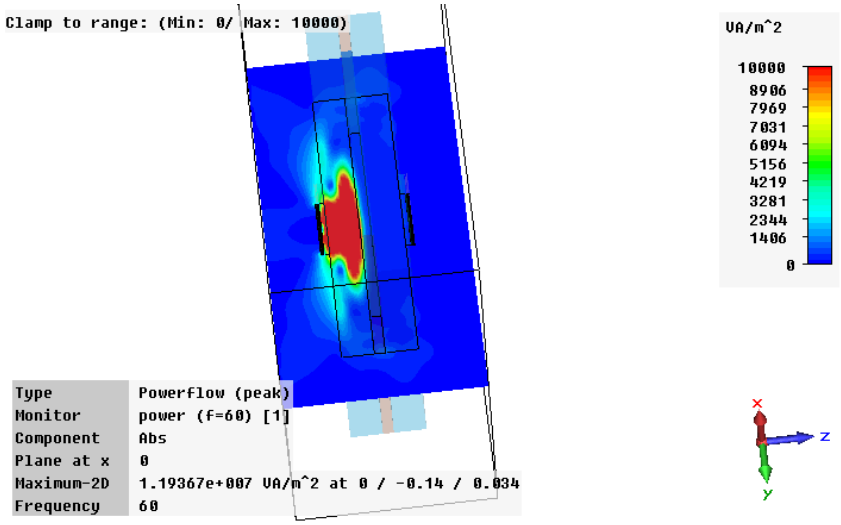

FIGURE 4.6: ABSOLUTE POWER FLOW DISTRIBUTION WHEN THE TANK IS FILLED WITH A 3% GLUCOSE SOLUTION

In this experiment, as in the waveguide power flow found in the waveguides (Section 3.3.1), the glucose solution absorbs the power.

The S-parameters for the assembly with different glucose concentrations are as follows:

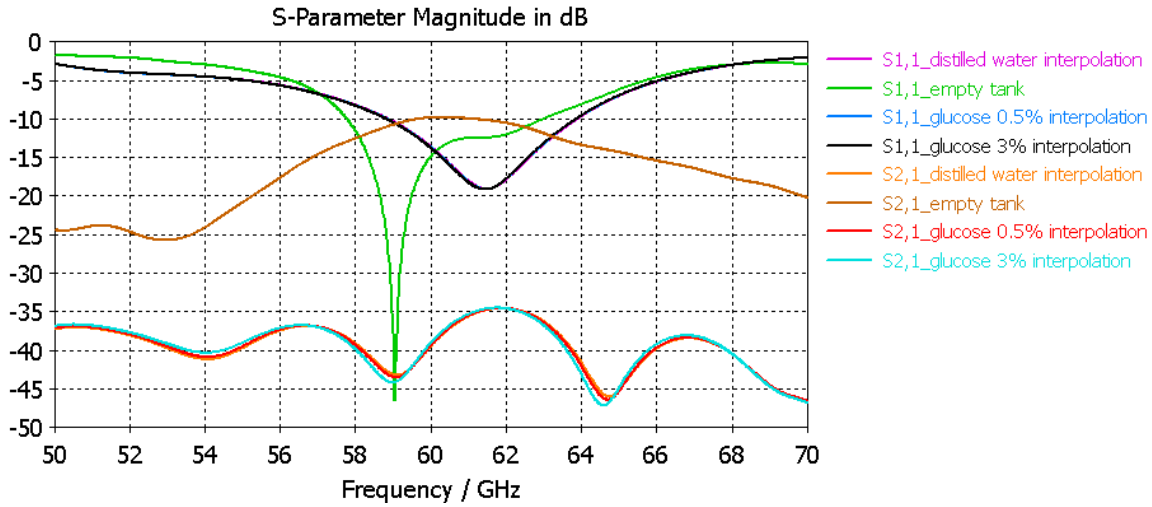

FIGURE 4.7: S-PARAMETERS FOR DIFFERENT CONCENTRATIONS AGAINST THE FREQUENCY

From the S-parameters (Fig. 4.7), it is possible to see that as in the waveguide case, the S_{11} and S_{21} are really similar for the different glucose concentrations. Furthermore, it can be seen how the solutions affect to the resonance peak of the antenna. The results of an empty tank present a resonance peak near 59 GHz and for the different glucose solutions, the resonance peak is near 61 GHz.

4.3.3. PARAMETRIC ANALYSIS OF DIFFERENT DIELECTRIC CONSTANT SOLUTIONS

The objective of this experiment is to take advantage of the changes in the resonance peak produced by the different concentrations inside the tank, and do a parametric analysis varying the dielectric constant of the solution between 1 and 15. To do this parametric analysis, the dielectric constant of the solutions has been defined as a parameter in the simulation options.

The results of the parameter analysis are as follows:

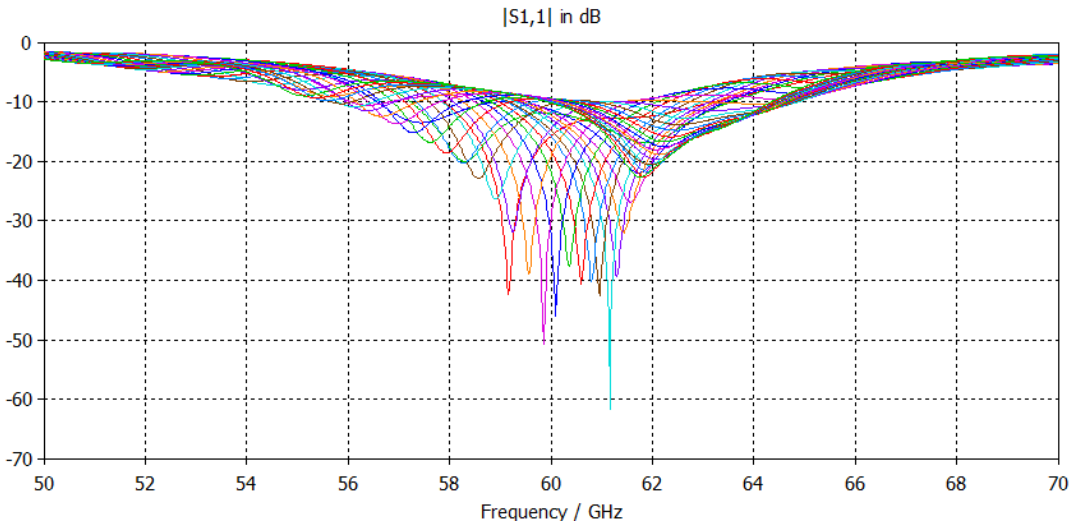

FIGURE 4.8: S11 AGAINST FREQUENCY FOR DIFFERENT SOLUTIONS WITH DIELECTRIC CONSTANT BETWEEN 1 AND 15

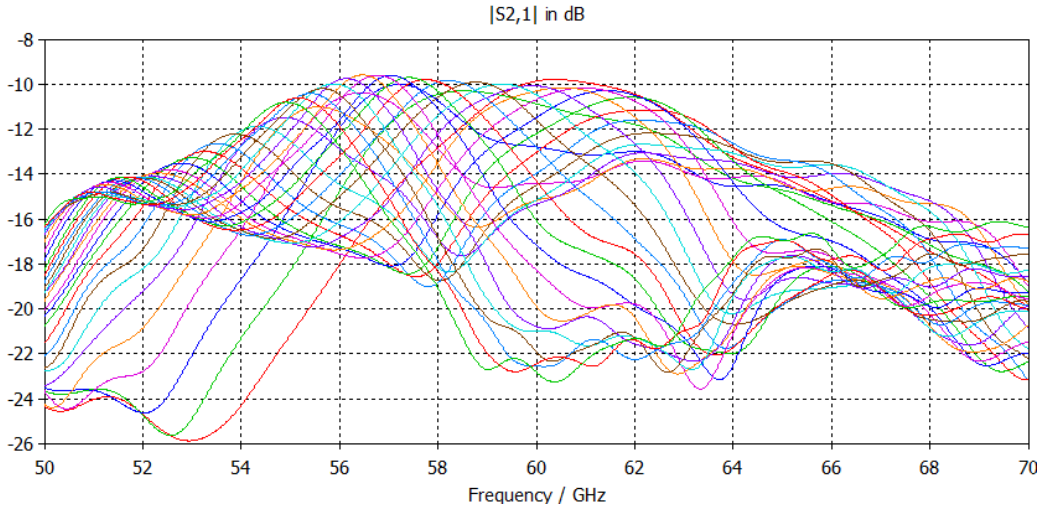

FIGURE 4.9: S21 AGAINST FREQUENCY FOR DIFFERENT SOLUTIONS WITH DIELECTRIC CONSTANT BETWEEN 1 AND 15

The results obtained in (Fig. 4.8 and 4.9) show too many curves and they are not easy to read. For this reason, another plot has been done taking the frequency of the resonance peaks of each solution and representing it against the permittivity values.

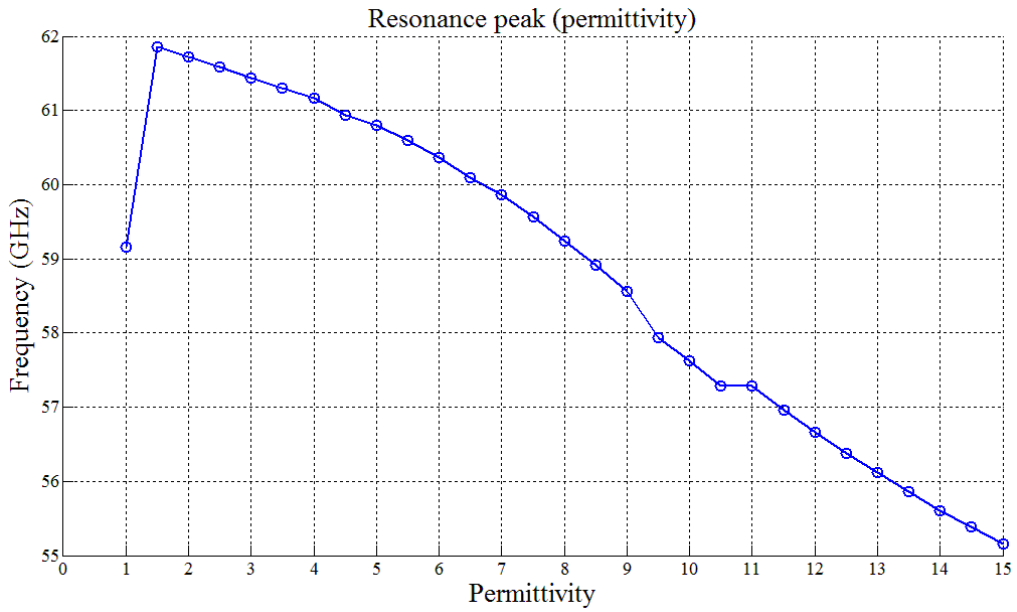

FIGURE 4.10: RESONANCE FREQUENCIES AGAINST THE PERMITTIVITY VALUES OF EACH SOLUTION

ε	Resonance peak (GHz)	ε	Resonance peak (GHz)	ε	Resonance peak (GHz)	ε	Resonance peak (GHz)
1	59.16	4.5	60.93	8	59.24	11.5	56.96
1.5	61.86	5	60.8	8.5	58.92	12	56.66
2	61.72	5.5	60.6	9	58.56	12.5	56.38
2.5	61.58	6	60.36	9.5	57.94	13	56.12
3	61.44	6.5	60.1	10	57.62	13.5	55.86
3.5	61.3	7	59.86	10.5	57.28	14	55.6
4	61.16	7.5	59.56	11	57.28	14.5	55.38
						15	55.16

TABLE 4.2: VALUES OF THE RESONANCE PEAK FOR EACH SOLUTION

The results obtained in (Fig. 4.10) and the specific values in (Table 4.2) are really useful for the determination of the permittivity of an unknown solution. If one experiment is based in the antenna setup and the resonance peak is known, using the values of (Fig. 4.10) we can know the dielectric constant of the solution placed inside the tank.

Therefore, this assembly can be used, not only to determine the glucose concentration, but also to determine the dielectric constant for other solutions. Furthermore, this same analysis can be done for the waveguide structure.

4.3.4. ANTENNA AND WAVEGUIDE STRUCTURES SENSITIVITY COMPARISON

The aim of this experiment is to compare the sensitivity of the antenna and the waveguide structures and evaluate it for both methods. This comparison method is based in the Root-mean-square deviation.

$$difference = \sqrt{\frac{\sum_i (|a(i) - b(i)|^2)}{\Delta f}} \tag{4.1}$$

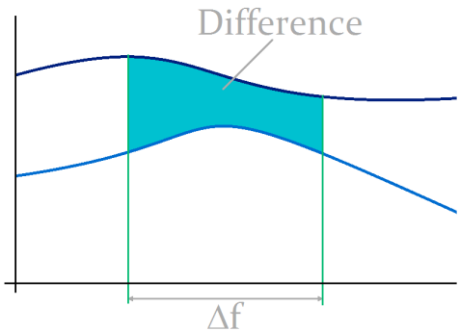

FIGURE 4.11: PARAMETERS OF THE ROOT-MEAN-SQUARE DEVIATION

This equation is useful to find the difference between two curves, a and b, in a specific frequency range, Δf. In this experiment, the comparison has been done between the 0.5% glucose solution and 3% glucose solution results for both assemblies. These differences are compiled in a table (Table 4.3) for two frequency ranges, the full frequency range and the maximum sensitivity range. This range of maximum sensitivity is a frequency range that contains the frequencies where the difference between the two curves is maximum.

To find the difference between the curves, different simulations had been done in order to get the necessary values to do the comparison.

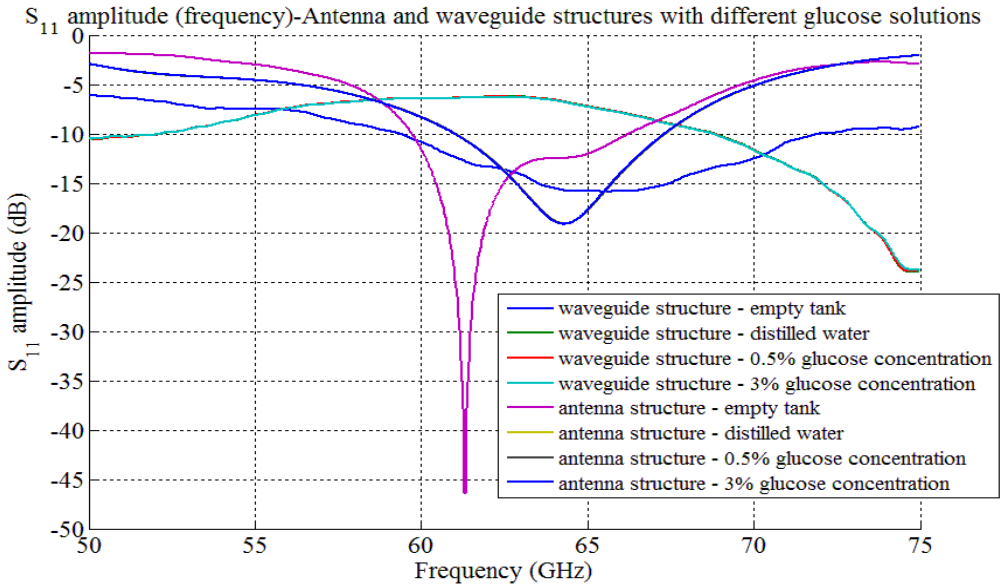

FIGURE 4.12: S11 AGAINST THE FREQUENCY FOR ANTENNA AND WAVEGUIDE STRUCTURES AND DIFFERENT SOLUTIONS

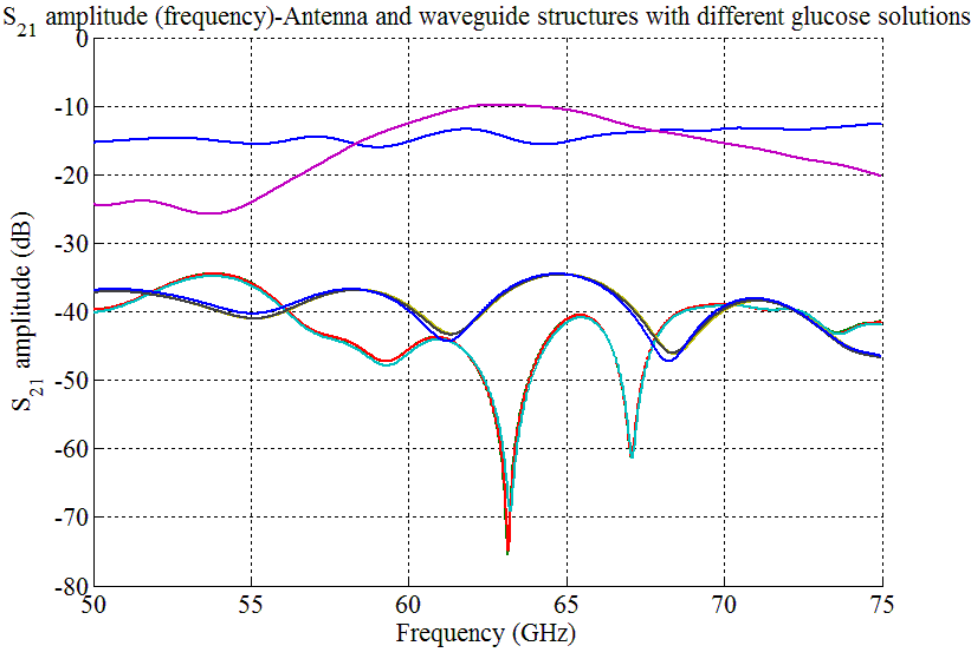

FIGURE 4.13: S21 AGAINST THE FREQUENCY FOR ANTENNA AND WAVEGUIDE STRUCTURES AND DIFFERENT SOLUTIONS, THE LEGEND IS THE SAME THAN THE LEGEND OF (FIG. 4.12)

	S_{11}		S_{21}	
	Wg	**Ant**	**Wg**	**Ant**
Δf = 50 - 75	0.06 dB	0.03 dB	0.70 dB	0.50 dB
Δf =maximum sensitivity	0.04 dB	0.06 dB	0.35 dB	0.35 dB

TABLE 4.3: DIFFERENCES BETWEEN THE 3% GLUCOSE CONCENTRATION AND THE 0.5% GLUCOSE CONCENTRATION FOR TWO DIFFERENT FREQUENCY RANGES.

In the table (table 4.3) the ranges of maximum sensitivity for the waveguide and the antenna are not the same.

	S_{11}	S_{21}
Waveguide structure	59 GHz - 63 GHz	67.8 GHz - 67.9 GHz
Antenna structure	60 GHz - 61 GHz	63.1 GHz - 63. 17 GHz

TABLE 4.4: RANGES OF MAXIMUM SENSITIVITY FOR BOTH STRUCTURES

From the table (Table 4.3), it is possible to see that, for S_{11}, the sensitivity of the waveguide structure is better than sensitivity of the antenna structure for all the frequency range. However, for the range of maximum sensitivity, the antenna structure has better sensitivity than the waveguide structure.

For S_{21}, in all frequency range the waveguide structure is the most sensitive method, but for the frequency range of maximum sensitivity, both methods had more or less the same sensitivity.

The conclusions after the comparison between the two methods are that the waveguide structure has best sensitivity for all the frequency range but for maximum sensitivity ranges is better to use the antenna structure.

4.3.5. TRL CALIBRATION FOR THE ANTENNA STRUCTURE

The aim of this experiment is to use the TRL calibration and the NRW method to obtain the permittivity and permeability of a solution placed inside the tank. The methodology to do this experiment presents the same steps than the methodology used in (Fig. 3.12).

In this experiment, the assembly used to test this method is a simplified model.

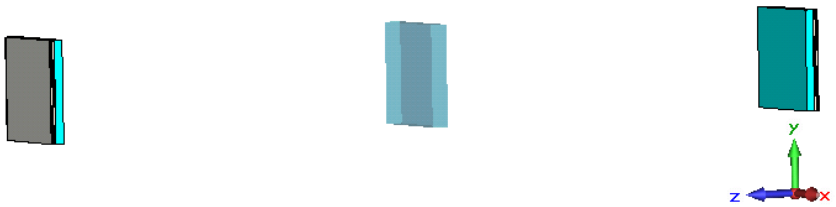

FIGURE 4.14: SIMPLIFIED MODEL OF THE ANTENNA STRUCTURE

This simplified model consists of two antennas separated by 49 mm and 1 mm slab of acrylic between them. The distance between the slab and the antennas correspond to the focal length of the microstrip antenna, 24 mm. To determine this focal length several simulations had been done with the aim to place the sample where the waves are as flat as possible in order to simulate plane waves (Fig. 4.14).

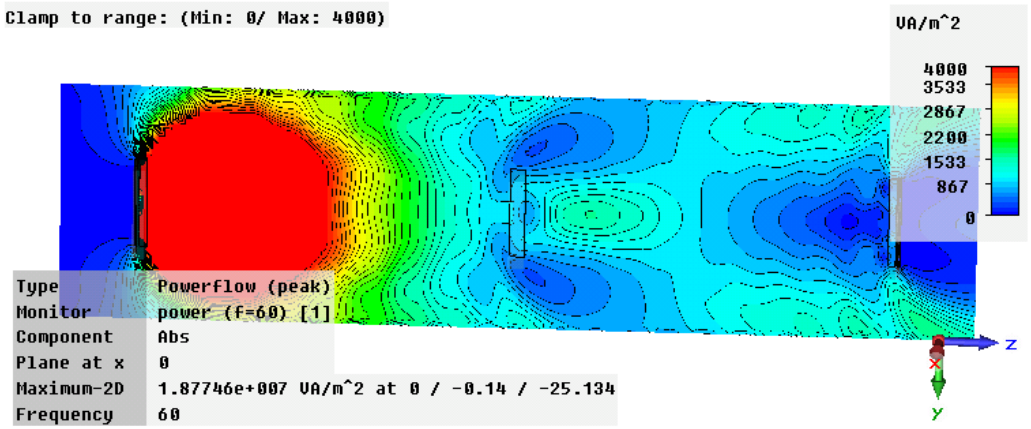

FIGURE 4.15: ABSOLUTE POWER FLOW DISTRIBUTION FOR A 12 MM DISTANCE BETWEEN THE TANK AND THE ANTENNAS

To simulate the Thru, the distance between the antennas has been selected to 48 mm, which correspond to two times the focal length of the antennas. To simulate the Line, the extra air gap between the antennas has been set as 1.25 mm, so the final distance between the antennas has been set to 49.25 mm

Finally, after the application of the calibration, the results are as follows:

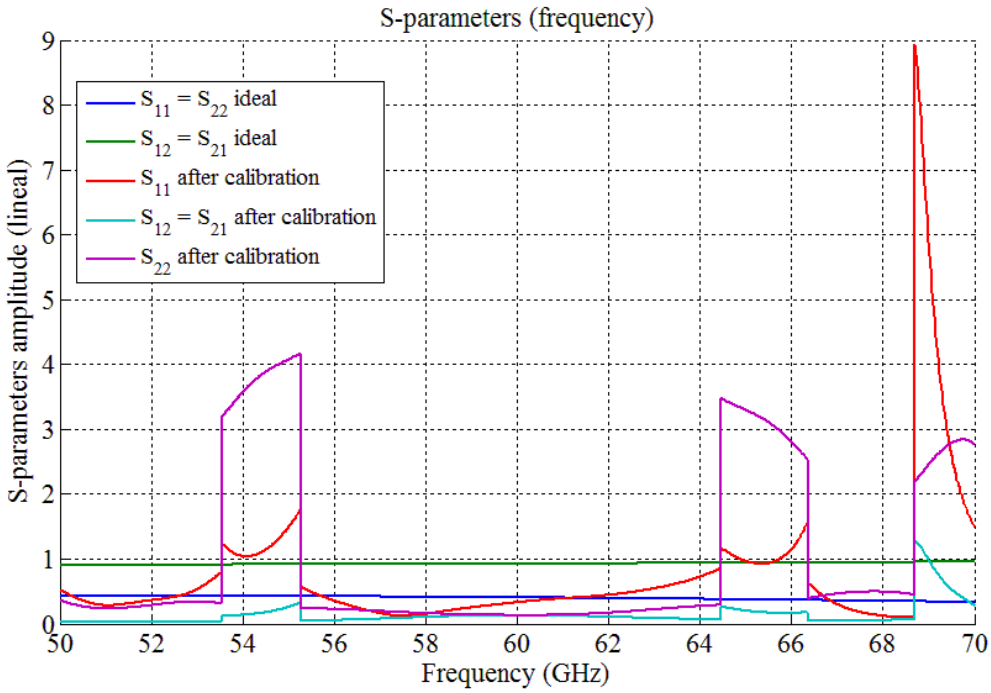

FIGURE 4.16: IDEAL AND AFTER CALIBRATION S-PARAMETERS AGAINST THE FREQUENCY

These S-parameters (Fig. 4.16) are not too good because they reach values greater than one. This error can be due to the fact that the waves are not plane at all. Nevertheless, a permittivity and permeability extraction using the NRW has been done.

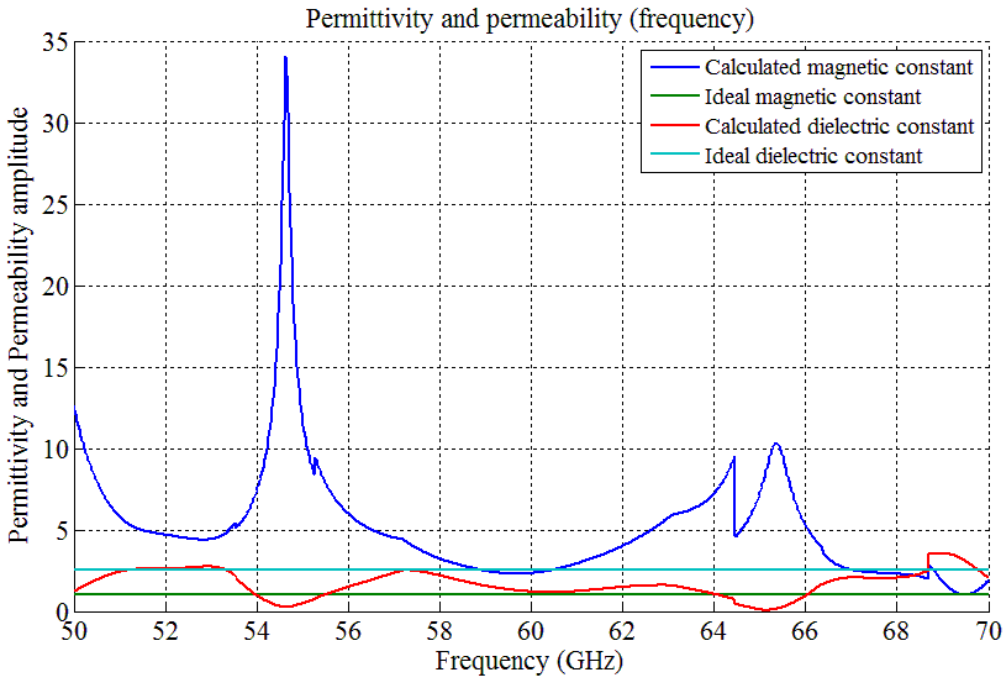

FIGURE 4.17: IDEAL AND CALCULATED (AFTER TRL AND NRW METHOD) PERMITTIVITY AND PERMEABILITY

As we could expect, the results are also not good, because of the accumulation of errors from (Fig. 4.16) due to the fact of non plane waves.

As the results were not good as expected, the next step to be consider is create our own calibration. However we did not have time to develop this idea at all because the equations involved were long and complicated. For this reason, the development of a new calibration has been left as a future work.

5. CONCLUSIONS

This thesis has presented a study of non-invasive techniques to determine the permittivity and permeability of a specific material. This study has analyzed using CST two different structures, the waveguide structure and the antenna structure in the frequency range between 50 GHz and 75 GHz.

The waveguide analysis has shown that the experimental and the simulation results are similar for the S_{11} parameter, but, in the case of the S_{21} parameter they differ. Furthermore, this analysis has exposed that plane waves are necessary to extract analytically the dielectric constant from the S-parameters using the TRL calibration and the Nicolson Ross Weir. For this reason, after the study of the waveguide structure, the thesis has focused in the study of the antenna structure.

The analysis of the microstrip antenna has presented that different solutions with different dielectric constants make a change in the resonance frequency. So it is possible to use a parametric analysis, using the permittivity as a parameter, to know the resonance frequency for each solution. Subsequently, only with the resonance frequency, we can determine the dielectric constant of an unknown solution.

The study of the microstrip antenna has also presented that the TRL calibration does not work as we expected. Therefore, to make this method work is necessary more study and time and maybe a development of our own calibration system.

After the comparison of both methods, it can be concluded that the waveguide structure has best sensitivity for all the frequency range but for the ranges of maximum sensitivity, is better to use the antenna structure.

Finally, as a conclusion for our entire work, we can say that there is still a way to go to improve our non invasive technique. It would need more hours and more dedication to discover the best way to make this idea perfectly work. But I feel confident that this device is going to work and it will change the live of diabetic people making it much more pleasant and painless.

6. FUTURE WORK

The future work will consist of the development of our own calibration technique to remove the undesirable effects from the different structures' assembly. To develop this new calibration a known material will be placed between the antennas. The combination of the simulation S-parameters of all the assembly and the ideal parameters calculated from the NRW equations will provide the values of the error box matrix following the (Eq. 2.46). After determining the error box matrix, our own calibration will be complete. This calibration will be able to be used to determine the permittivity and permeability of different slabs of unknown materials.

Another part of the future work would consist of collecting and analyzing some experimental data using the antenna structure and the compare these results with the simulation results in orderto study and assess the waveguide structure.

Appendix A MORE RESULTS OF THE WAVEGUIDE STRUCTURE

A.1 EFFECT OF COMPONENTS ON S-PARAMETERS

The aim of this experiment is to study the effects of the different assembly's components in the S-parameters. For this reason, different simulations have been done for every added component.

SIMULATIONS PARAMETERS

- Frequency range: 50 GHz – 75 GHz.
- Boundary conditions: open space.
- Resolution: between 25 and 11 lines per wavelength (meshcells between 1,314,440 and 26,976,698).

MATERIALS

- Waveguides: Cooper (annealed).
- Rail line, rail carrier, nuts: PEC.
- Grid and waveguide support: plastic (ε=2).
- Tank: acrylic (ε=2.53), styrene (ε=2.725) and air (ε=1). The acrylic permittivity at 60 GHz can be found in [3] – acrylic (ε=2.53 tanδ=0.0119) - and the styrene permittivity is an approximation (ε=2.7225 tanδ=0.008).

RESULTS

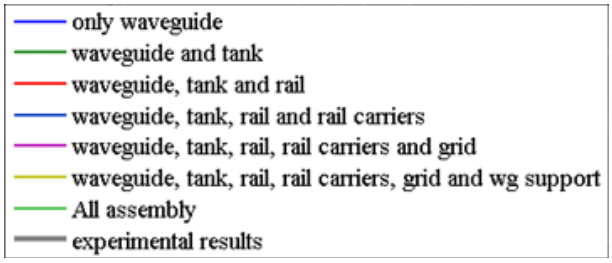

FIGURE A.1: LEGEND

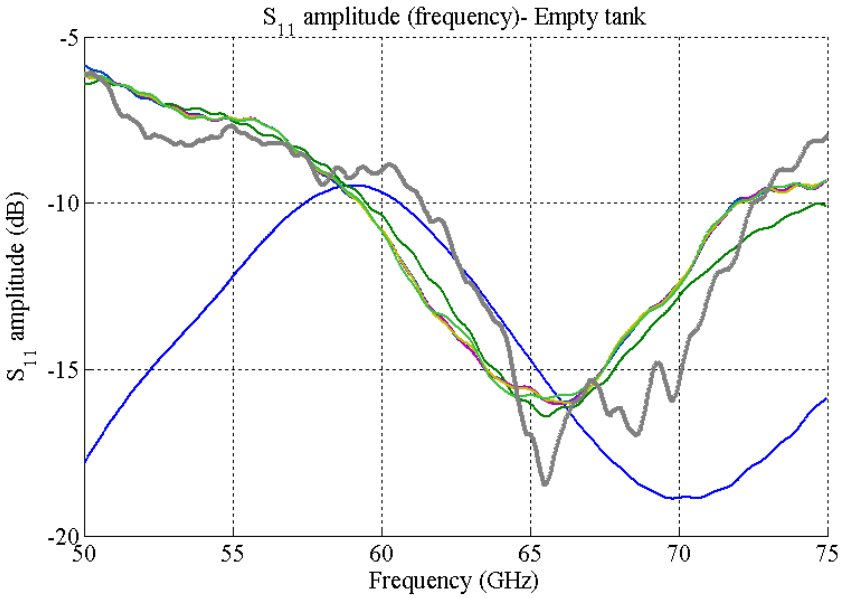

FIGURE A.2: S11 PARAMETER AGAINST FREQUENCY

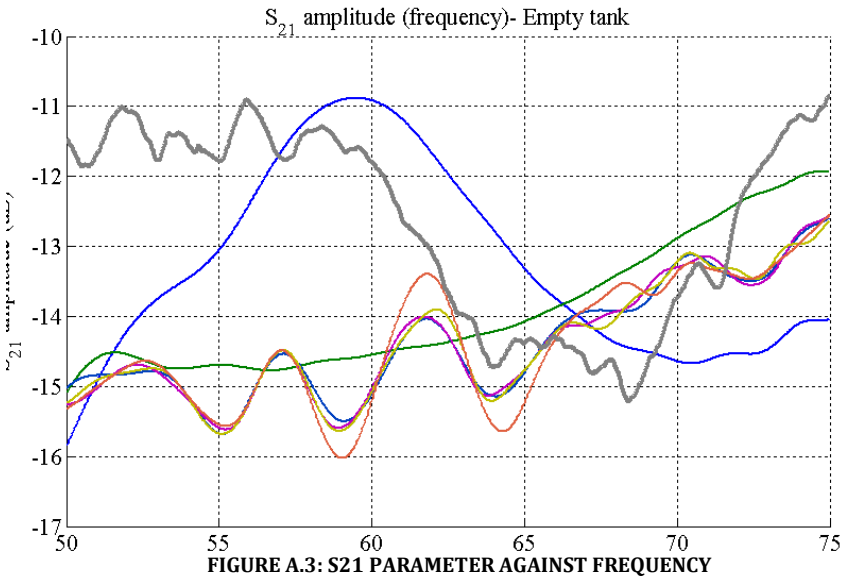

FIGURE A.3: S21 PARAMETER AGAINST FREQUENCY

EVALUATION OF THE RESULTS

From both figures (Fig. A.2 and A.3) it can notice that every added component creates a little change in the S-parameters. These figures also show that the experimental results and the simulated ones differ.

In (Fig. A.2), the shape of the experimental results and the simulation results curves is a bit similar. Nevertheless, in the (Fig. A.3) the shape of the experimental results and the simulated ones differ.

A.2 AIR GAP BETWEEN WAVEGUIDES

The aim of this experiment is to study the changes in the S-parameters due to the increasing gap between waveguides. The assembly of this experiment is showed in the following figure (Fig. A.4).

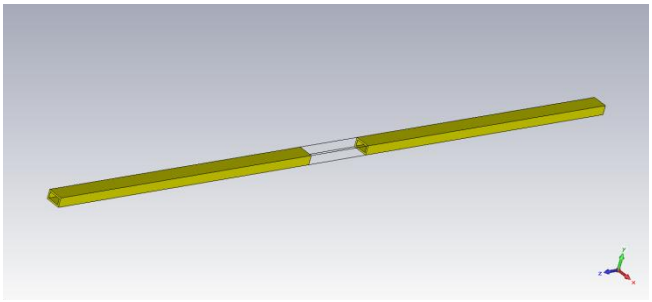

FIGURE A.4: ASSEMBLY OF THIS EXPERIMENT

SIMULATIONS PARAMETERS

- Frequency range: 50 GHz – 75 GHz
- Boundary conditions: open space
- Symmetry planes: YZ-magnetic, XZ-electric
- Resolution: 10 lines per wavelength, 231,840 meshcells

MATERIALS

- Waveguides: Cooper (annealed)

RESULTS

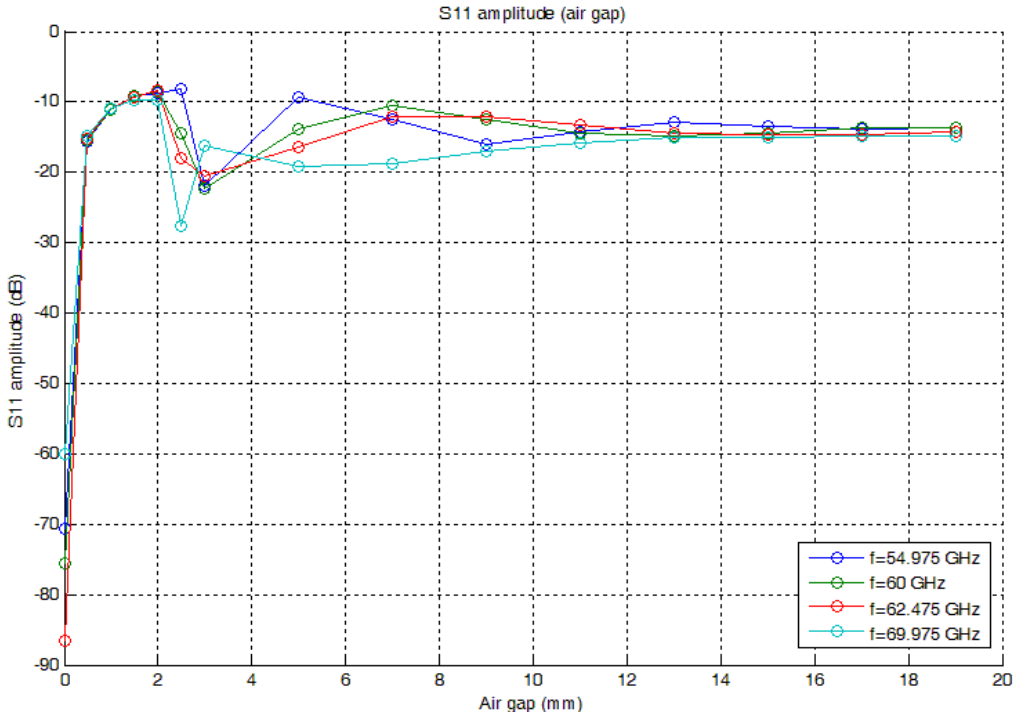

FIGURE A.5: S_{11} AGAINST THE DISTANCE BETWEEN WAVEGUIDES FOR DIFFERENT FREQUENCIES

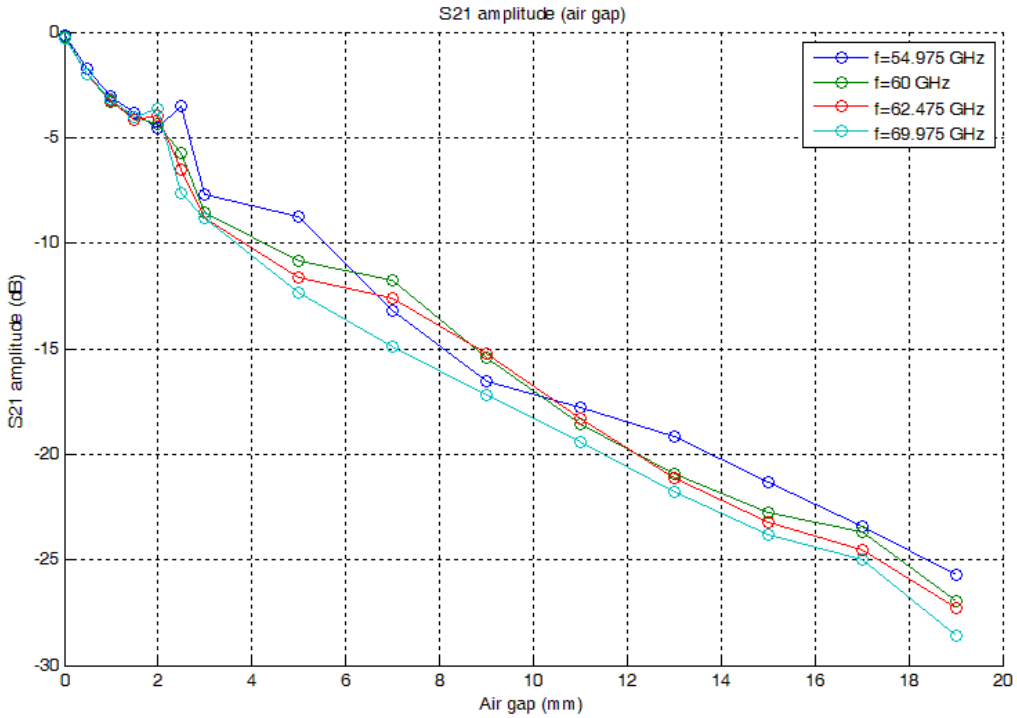

FIGURE A.6: S_{21} AGAINST THE DISTANCE BETWEEN WAVEGUIDES FOR DIFFERENT FREQUENCIES

EVALUATION OF THE RESULTS

From the figures, we can see that for bigger gaps the amplitude of S_{21} is lower. This result is an expected result because if the gap is big, logically, the transmission signal is weak. Regarding to S_{11}, if we take a look to the figure 18, we can see that S_{11} is always around -15 dB, except for distances less than 12 mm approximately.

If we focus on the S_{21} graph, we can see that at 7 mm, our tank thickness, the S_{21} parameters have values around -16 dB, these values are far from the ideal value that should be 0 dB.

Appendix B MORE RESULTS OF THE ANTENNA STRUCTURE

B.1 TWO ANTENNAS AND THIN TANK STUDY

The aim of this experiment is to study the S-parameters of the different glucose concentrations using the following structure:

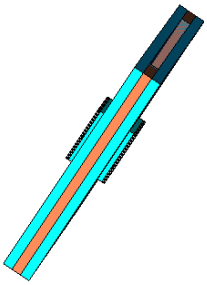

FIGURE B.1: CIRCLE PATCH ANTENNA AND THIN TANK STRUCTURE

SIMULATIONS PARAMETERS

- Frequency range: 50 GHz – 75 GHz
- Boundary conditions: open space 5mm add space.
- Resolution: 20 lines per wavelength

MATERIALS

- Ground plane: PEC
- Substrate: Rogers RT5880 (εr=2.2)
- Microstrip line: PEC
- Substrate: Rogers RT5880 (εr=2.2)
- Patch: PEC
- Plastic cover: ABS (εr=2.2)
- Tank: acrylic (ε=2.53 tanδ=0.0119), styrene (ε=2.575 tanδ=0.008) and interpolated glucose solutions.

RESULTS

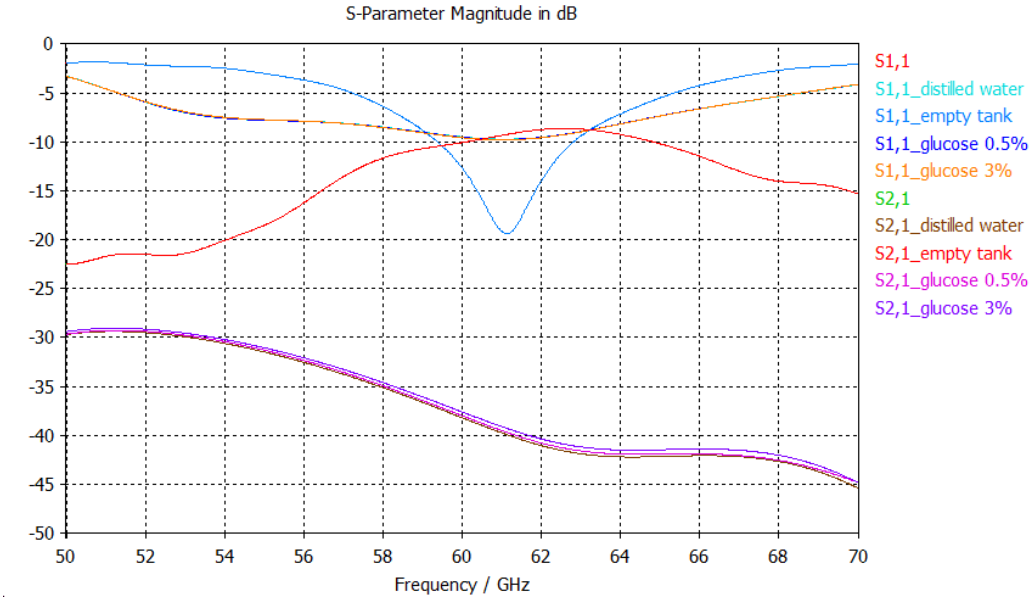

FIGURE B.2: S-PARAMETERS AGAINST FREQUENCY

EVALUATION OF THE RESULTS

If we compare this figure (Fig. B.2) with (Fig. 4.7), we can see that in (Fig. B.2), we do not have any resonant peaks for S_{21}. Furthermore, in (Fig. B.2), the values are bigger than the values in (Fig. 4.7). Finally, for the S_{11} parameters of the glucose concentrations, it can be noticed that with this thin tank, there are not any strong peak as in the other case.

Appendix C MATLAB CODES

C.1 TRL CALIBRATION

```
function [s11dut,s21dut,s12dut,s22dut] =
calibration(s11re,s11im,s21re,s21im,z0)

%Load the Thru and Line parameters
T11re=load('D:\Helena\Results\Antenna\Calibration\thru\s11re18mm.txt');
T11im=load('D:\Helena\Results\Antenna\Calibration\thru\s11im18mm.txt');
T21re=load('D:\Helena\Results\Antenna\Calibration\thru\s21re18mm.txt');
T21im=load('D:\Helena\Results\Antenna\Calibration\thru\s21im18mm.txt');
L11re=load('D:\Helena\Results\Antenna\Calibration\Line\s11re18mm.txt');
L11im=load('D:\Helena\Results\Antenna\Calibration\Line\s11im18mm.txt');
L21re=load('D:\Helena\Results\Antenna\Calibration\Line\s21re18mm.txt');
L21im=load('D:\Helena\Results\Antenna\Calibration\Line\s21im18mm.txt');

l=1.25e-3;
z0=1;
E=zeros(1001,1);
ABCDe=zeros(2,2,1001);
ABCDm=zeros(2,2,1001);
ABCDdut=zeros(2,2,1001);
Adut=zeros(1001,1);
Bdut=zeros(1001,1);
Cdut=zeros(1001,1);
Ddut=zeros(1001,1);

%CALIBRATION

%Thru
T11=T11re(1:end,2)+1i*T11im(1:end,2);
T21=T21re(1:end,2)+1i*T21im(1:end,2);

%Line
L11=L11re(1:end,2)+1i*L11im(1:end,2);
L21=L21re(1:end,2)+1i*L21im(1:end,2);

%ERROR BOX MATRIX

%Unknowns s11,s12=s21, s22, g, Gl
E1=(L21.^2+T21.^2-(T11-L11).^2+sqrt((L21.^2+T21.^2-(T11-L11).^2).^2-
4*L21.^2.*T21.^2))./(2*L21.*T21);
E2=(L21.^2+T21.^2-(T11-L11).^2-sqrt((L21.^2+T21.^2-(T11-L11).^2).^2-
4*L21.^2.*T21.^2))./(2*L21.*T21);
g1=-1/l*log(E1);
g2=-1/l*log(E2);

for R=1:1001
    if ((real(g1(R))>=0)&&(imag(g1(R))>=0))
        E(R)=E1(R);
    elseif ((real(g2(R))>=0) && (imag(g2(R))>=0))
        E(R)=E2(R);
```

```
    elseif (real(g2(R))>=0)
        disp('Error1');
        E(R)=E2(R);
    elseif (real(g1(R))>=0)
        disp('Error1');
        E(R)=E1(R);

    else
        disp('Error');
    end
end
s22e=(T11-L11)./(T21-L21.*E);
s11e=T11-s22e.*T21;
s12e=sqrt(T21.*(1-s22e.^2));
[Ae,Be,Ce,De] = s2abcd (s11e,s12e,s12e,s22e,z0);

%MATRIX FOR ALL THE ASSEMBLY

s11m=s11re(1:end,2)+1i*s11im(1:end,2);
s21m=s21re(1:end,2)+1i*s21im(1:end,2);
[Am,Bm,Cm,Dm] = s2abcd (s11m,s21m,s21m,s11m,z0);

%MATRIX FOR THE DEVICE UNDER TEST

for R=1:1001
    ABCDe1=[Ae(R) Be(R);Ce(R) De(R)];
    ABCDm1=[Am(R) Bm(R);Cm(R) Dm(R)];
    ABCDdut1=inv(ABCDe1)*ABCDm1*ABCDe1;
    Adut(R)=ABCDdut1(1,1);
    Bdut(R)=ABCDdut1(1,2);
    Cdut(R)=ABCDdut1(2,1);
    Ddut(R)=ABCDdut1(2,2);
    ABCDe(:,:,R)=ABCDe1;
    ABCDm(:,:,R)=ABCDm1;
    ABCDdut(:,:,R)=ABCDdut1;
end
[s11dut,s21dut,s12dut,s22dut]=abcd2s(Adut,Bdut,Cdut,Ddut,z0);
end
```

C.2 S-PARAMETERS TO ABCD PARAMETERS CONVERSION

```
function [A,B,C,D] = s2abcd(s11,s12,s21,s22,z0)
A = ((1+s11).*(1-s22)+s12.*s21)./(2*s21);
B = z0.*(((1+s11).*(1+s22)-s12.*s21)./(2*s21));
C = ((1-s11).*(1-s22)-s12.*s21)./(2*s21.*z0);
D = ((1-s11).*(1+s22)+s12.*s21)./(2*s21);
end
```

C.3 ABCD PARAMETERS TO S-PARAMETERS

```
function [s11,s21,s12,s22] = abcd2s(A,B,C,D,z0)
s11 = (A+B/z0-C*z0-D)./(A+B/z0+C*z0+D);
s12= 2.*(A.*D - B.*C)./(A+B/z0+C*z0+D);
s21=2./(A+B/z0+C*z0+D);
s22=(-A+B/z0-C*z0+D)./(A+B/z0+C*z0+D);
end
```

C.4 COMPARISON BETWEEN TWO CURVES

```
function [out] = comp(a,b,fmin,fmax)
res=zeros(6401,1);
freqa=zeros(6401,1);
sa=zeros(6401,1);
freqb=zeros(6401,1);
sb=zeros(6401,1);

siza=size(a);
sizb=size(b);

if siza(1)~=sizb(1)
    if siza(1)<sizb(1)
        freqa=spline(1:siza(1),a(1:end,1),1: (siza(1)-1)/(sizb(1)-
1):siza(1));
        freqa=freqa';
        sa=spline(1:siza(1),a(1:end,2),1: (siza(1)-1)/(sizb(1)-1):siza(1));
        sa=sa';
        freqb=b(1:end,1);
        sb=b(1:end,2);
        sizet=sizb(1);
    elseif sizb(1)<siza(1)
        freqb=spline(1:sizb(1),b(1:end,1),1: (sizb(1)-1)/(siza(1)-
1):sizb(1));
        sb=spline(1:sizb(1),b(1:end,2),1: (sizb(1)-1)/(siza(1)-1):sizb(1));
        freqa=a(1:end,1);
        sa=a(1:end,2);
        sizet=siza(1);
    end
else
    freqa=a(1:end,1);
    sa=a(1:end,2);
    freqb=b(1:end,1);
    sb=b(1:end,2);
    sizet=siza(1);
end
p=0;
for R=1:sizet
    if ((freqa(R)>=fmin) && (freqa(R)<=fmax))
        p=p+1;
        res(p)=abs(sa(R)-sb(R))^2;
    end
end
```

```
total=sum(res(1:end));
out=sqrt(total/p);
end
```

REFERENCES

[1] M. Harris, P. Zimmet, "Classification of diabetes mellitus and other categories of glucose intolerance", *International Textbook of Diabetes Mellitus*, 2nd Edition, John Wiley and Sons, 1997.

[2] M. B. Davidson, "Diabetes Mellitus- Diagnosis and Treatment", 3rd edition, Churchill Livingstone, 1991.

[3] International Diabetes Federation, "IDF Diabetes Atlas 2012", 5th edition, 2012. Available from: http://www.idf.org/diabetesatlas. Accessed: August 2013.

[4] G. M. Grodsky *et al.*, "Metabolic and Underlying Causes of Diabetes Mellitus", *Diabetes*, vol. 31, suppl 1, 1982.

[5] J. Wang, "Glucose Biosensors: 40 Years of Advances and Challenges", *Electmanalysis*, vol. 13, no. 12, pp. 983-988, 2001.

[6] M. M. Rahman *et al.*, "A Comprehensive Review of Glucose Biosensors Based on Nanostructured Metal-Oxides", *Sensors* ,2010, 10, 4855-4886.

[7] Cuiñas; M. García, "Permittivity and conductivity measurements of building materials at 5.8 GHz 41,5 GHz", *Wireless Personal Communications*, vol. 20, pp. 93-100, 2002.

[8] K. Sato *et al.*, "Measurements of reflection and transmissions characteristics of interior structures of office building in the 60 GHz band", *IEEE transactions on antennas and propagation*, vol. 45, pp. 1783-1792, 1997.

[9] R. Pottel *et al.*, "The dielectric permittivity spectrum of aqueous colloidal phospholipid solutions between 1 KHz and 60 GHz, *Biophysical Chemistry*, vol. 19, pp. 233-244, 1984.

[10] Z. Abbas *et al.*, "RDWG technique of determination of moisture content in Oil Palm Fruits", *Eur. Phys. J. Appl*, Phys., pp. 207-210, 2007.

[11] V. V. Meriakri *et al.*, "Dielectric properties of glucose solutions in the millimetre-wave range and control of glucose content in blood", *Measurement science and technology*, vol. 18, pp. 1-6, 2007.

[12] Y. Nikawa, T. Michiyama, "Blood-Sugar Monitoring by Reflection of Millimeter Wave", *Proceedings of Asia-Pacific Microwave Conference*, pp. 1-4, 2007.

[13] R. S. Rao, "Electromagnetic Waves and Transmission Lines", 1st edition, PHI Learning, 2012.

[14] D. M. Pozar, "Microwave Engineering", 2nd edition, John Wiley & sons, 1998.

[15] S. Ramo; J.R. Whinnery; T. V. Duzer, "Fields and Waves in Communication Electronics", 3rd edition, John Wiley & sons, 1965.

[16] S. J. Orfanidis, "Electromagnetic Waves and Antennas", 1996. Available from: http://www.ece.rutgers.edu/~orfanidi/ewa. Consulted: August 2013.

[17] D. K. Cheng, "Fundamentals of Engineering Electromagnetics", 1st edition, Addison-Wesley, 1998.

[18] M.N.O. Sadiku, "Elements of electromagnetics", 5th edition, OUP USA, 2010.

[19] D. G. Fang, "Antenna Theory and Microstrip Antennas", 1st edition, CRC Press, 2010.

[20] C. A. Balanis, "Modern antenna Handbook",1st edition, John Wiley & sons, 2008.

[21] D. M. Pozar, "Microstrip antennas", *IEEE Proceeding*, vol. 80, pp.79 -91, 1992.

[22] R. C. Johnson, "Antenna Enginnering Handbook", 3rd edition, McGraw Hill, 1993.

[23] S. Drabowitch, A. Papiernik, "Modern Antennas",2nd ed., Springer, 2005.

[24] G. Ramesh, "Microstrip antenna design handbook", Artech house, 2001.

[25] "IEEE Standard Definitions of Terms for Antenna", *Antennas and Propagation*, IEEE Transactions on, vol. 17, Issue 3, pp. 262-269, 1969.

[26] C. A. Balanis, "Antenna Theory: Analysis and Design", 2nd edition, John Wiley & sons, 1982.

[27] T. S. Bird, "Definition and Misuse of Return Loss", *IEEE Antennas & Propagation Magazine*, vol. 51, pp. 166-167, 2009.

[28] J. Choma, Jr., "Electrical Networks: Theory and Analysis", John Wiley & sons, 1985.

[29] Rolfes and B. Schiek, "Calibration methods for microwave free space measurements", *Advances in Radio Science*, pp. 19-25, 2004.

[30] D. K. Ghodgaonkar; V. V. Varadan., "Free-Space Measurement of Complex Permittivity of Magnetic Materials at Microwave Frequencies", *IEEE Transactions on Instrumentation and Measurement*, Vol. 19, No. 2, April 1990.pp. 387 – 394.

[31] J.B. Jarvis *et al.*, "Measuring the Permittivity and Permeability of Lossy Materials: Liquids, -Metals , Building Materials and Negative-Index Materials", *National Institute of Standards and Technology*, 2005.

[32] W. B. Weir, "Automatic Measurement of Complex Dielectric Constant and Permeability at Microwave Frequencies", *Proceedings of the IEEE*, vol. 62, no. 1, pp. 33-36, 1974.

[33] M. Nicolson, G. F. Ross, "Measurement of the Intrinsic Properties of Materials by Time-Domain Techniques", *IEEE Transactions on Instrumentation and Measurement*, vol. im19, no. 4. pp. 377-382, 1970

[34] Luis M. Correia and Paulo O. Frances, "Estimation of Materials Characteristics from Power Measurements at 60 GHz", *Personal, Indoor and Mobile Radio Communications*, 1994.

[35] V. Meriakri *et al.*," Dielectric Properties of Water Solutions with Small Content of Sugar and Glucose in the Millimeter Wave Band and the Determination of Glucose in Blood", *Proc. ISEMA-2005*, pp. 65-72, 2005.